https://doi.org/10.5194/egusphere-2025-1164
Preprint. Discussion started: 3 April 2025

Seasonal evolution of snow density and its impact on thermal regime of sea ice during the MOSAiC expedition

Yubing Cheng[1], Bin Cheng[2], Roberta Pirazzini[2], Amy R. Macfarlane[3,4], Timo Vihma[2], Wolfgang Dorn[1], Ruzica Dadic[5], Martin Schneebeli[5], Stefanie Arndt[6], and Annette Rinke[1]

[1]Alfred Wegener Institute, Helmholtz Centre for Polar and Marine Research, Potsdam, Germany
[2]Finnish Meteorological Institute, Helsinki, Finland
[3]The Arctic University of Norway UiT, Tromsø, Norway
[4]Northumbria University, Newcastle Upon Tyne, UK
[5]WSL Institute for Snow and Avalanche Research SLF, Davos Dorf, Switzerland
[6]Alfred Wegener Institute, Helmholtz Centre for Polar and Marine Research, Bremerhaven, Germany

Correspondence to: Bin Cheng (bin.cheng@fmi.fi)

Abstract. Snow density is a crucial parameter for snow and sea ice modelling at the physical process level. The seasonal evolution of surface (top 3 cm) and bulk (entire layer) snow densities observed during MOSAiC expedition were investigated and used to access several snow density schemes. A numerical snow and sea ice model was applied to simulate the impact of snow density on the thermal regime of sea ice during the period when snow was dry. The constant snow densities of 348 kg/m³, 308 kg/m³ and 487 kg/m³ were derived from linear regression of snow water equivalent (SWE) versus snow depth, using samples collected during the entire MOSAiC period, the winter-spring period (October–May), and summer-autumn period (June- September), respectively. The examined snow density schemes produced mean snow densities consistent with MOSAiC observations; however, none of the schemes adequately captured the observed temporal variability. The modelled mean surface temperature and ice thickness were linearly related to the snow density, whereas the modelled mean in-snow and in-ice temperatures had linear inverse relationships with the snow density. The impacts of time-dependent snow density on snow and ice thermodynamic regimes were stronger than in the model runs using constant snow density. Model sensitivity experiments revealed contrasting responses of the snow and ice system to changes in snow density and precipitation. Increased snow density decreased snow and ice temperatures, promoting ice growth, while increased precipitation led to warmer snow and ice temperatures and reduced ice thickness.

1 Introduction

Snow on top of sea ice is an important component of the marine Arctic climate system. First, snow is a strong reflector of solar radiation, with a surface albedo much higher than that for bare ice (Perovich and Polashenski, 2012). This keeps the surface temperatures lower in spring and autumn and reduces the melt in late spring and early summer. Second, snow is a good insulator, having a heat conductivity of only approximately 10-20 % of that of sea ice (Sturm et al., 2002, Macfarlane et al., 2024). Hence, in winter the heat flux from the relatively warm ocean to the cold atmosphere is much smaller when sea ice is

https://doi.org/10.5194/egusphere-2025-1164
Preprint. Discussion started: 3 April 2025

covered by snow resulting in a reduction in the ice growth rate (Merkouriardi et al., 2017). Third, snow has a positive contribution to the sea-ice mass balance via snow-to-ice transformation to increase the ice thickness. This occurs when the ice surface is flooded under a heavy snowpack and slush freezes to form snow ice (Provost et al., 2017) or when melt water or rain percolates to the snow-ice interface and refreezes there to form superimposed ice (Cheng et al., 2006). For multi-year sea ice in the Arctic, a surface scattering layer (SSL) may exist on top of sea ice during and after summer (Macfarlane et al., 2023b; Smith et al., 2022). The origin of the SSL is largely ice, although it is visually like a snow layer. It has a surface albedo greater than that of bare ice but less than that of snow.

Snow density is an important factor in all of the above. Snow density affects the thermal properties of the snowpack, as for instance new, dry, low-density snow has a much lower heat conductivity than wet, high-density snow (Macfarlane et al., 2023c). Snow density determines the mass of a snowpack at a certain depth and accordingly affects the snow-ice formation ice by submerging the sea ice surface and causing flooding. Furthermore, snow density influences the formation of superimposed ice by affecting the percolation of meltwater to the snow-ice interface. Additionally, the lower the snow density, the weaker the wind required for erosion (He and Ohara, 2017). Lighter snow tends to be more easily subjected to drifting and blowing, which enhances sublimation (Sigmund et al., 2022) and can act as a source of fine-mode salt aerosols, serving as cloud condensation nuclei (Gong et al., 2023). In the satellite retrieval of sea ice thickness, snow density is critically important (Kern et al., 2015). Vertical snow density gradients and/or volume scattering in the snow influence the radar signal: a 30% uncertainty in snow density can translate into a roughly 0.3 m uncertainty in the satellite-retrieved sea ice thickness (Kern et al., 2015).

After snowfall, snow density begins to evolve due to snow metamorphism, which results in stratigraphic layering, compaction, and densification (Bormann et al., 2013; Helfricht et al., 2018; Judson and Doesken, 2000). The factors controlling snow metamorphosis can be divided into dynamic and thermodynamic factors. The dynamic factors are due to wind and snowfall. Wind generates pressure forces acting on snow grains, which result in the breaking of fine structures and rounding of the grains (King et al., 2020). This increases snow density, as the rounded grains are packed more compactly. Snowfall typically reduces the bulk density of the snowpack, as the newly fallen snow usually has a lower density than older snow (Sturm and Holmgren, 1988). The major challenge in quantifying the role of snowfall in snow metamorphism, snow depth and ice mass balance beneath the snow layer is that the temporal and spatial variations of snowfall are often poorly understood. Measurements of the total local seasonal snowfall tend to differ from each other, depending on the instrument used (Matrosov et al., 2022). Thermodynamic metamorphosis is caused by densification due to melting and refreezing as well as by sublimation, transport of water vapor, and condensation (Jafari et al., 2020; Nicolaus et al., 2022). The water vapor transport may be generated by a thermal gradient through the snowpack or in the range of individual snow grains.

Even if the microscale physics of the factors controlling the snow density is reasonably well understood (Keenan, et al., 2021), major challenges remain in the presentation of the processes in climate models. Those can only resolve bulk properties of the snowpack, such as its depth and temperature. Various snow-density parameterizations have already been developed (e.g., Essery et al., 2013, Keenan, et al., 2021). In most climate models involved in the Snow Model Intercomparison Project

https://doi.org/10.5194/egusphere-2025-1164
Preprint. Discussion started: 3 April 2025

(SNOW-MIP), snow density is either constant or depends on mechanical compaction and snow age (Menard et al., 2021). However, limited and sparse data availability from the central Arctic has hindered a comprehensive assessment of the snow density on sea ice and its dependence on variables resolved by climate models.

In this study, we investigate the seasonal evolution of snow density, as observed during the Multidisciplinary drifting Observatory for the Study of Arctic Climate (MOSAiC) expedition (Shupe et al., 2020). We address snow density for the surface layer (top 3 cm) and for the bulk snowpack. Our objectives are to find out (1) how snow density is affected by air temperature over the annual cycle, (2) how snow density is affected by wind during the winter-spring period, (3) how the simulated thermal evolution of snow and ice varies depending on the applied snow density scheme, and (4) how snowfall impacts the thermal evolution of the previously deposited snow and underlying ice.

2 Data and methods

The MOSAiC expedition to the central Arctic started in October 2019 and lasted until September 2020. The MOSAiC ice camp (RV *Polarstern*) drift started from the marginal ice zone (MIZ) in the eastern Amundsen Basin and ended in the Fram Strait (Fig. 1). The expedition was divided into five legs. Legs 1 to 3 were operated along a continuous ice camp (central observatory 1, CO1) between October 2019 and mid-May 2020. Leg 4 between June and August 2020 (central observatory 2, CO2). Leg 5 was set-up after a complete relocation of RV Polarstern back up to the central high-Arctic (central observatory 3, CO3). The complete drift trajectory can be seen in Fig. 1.

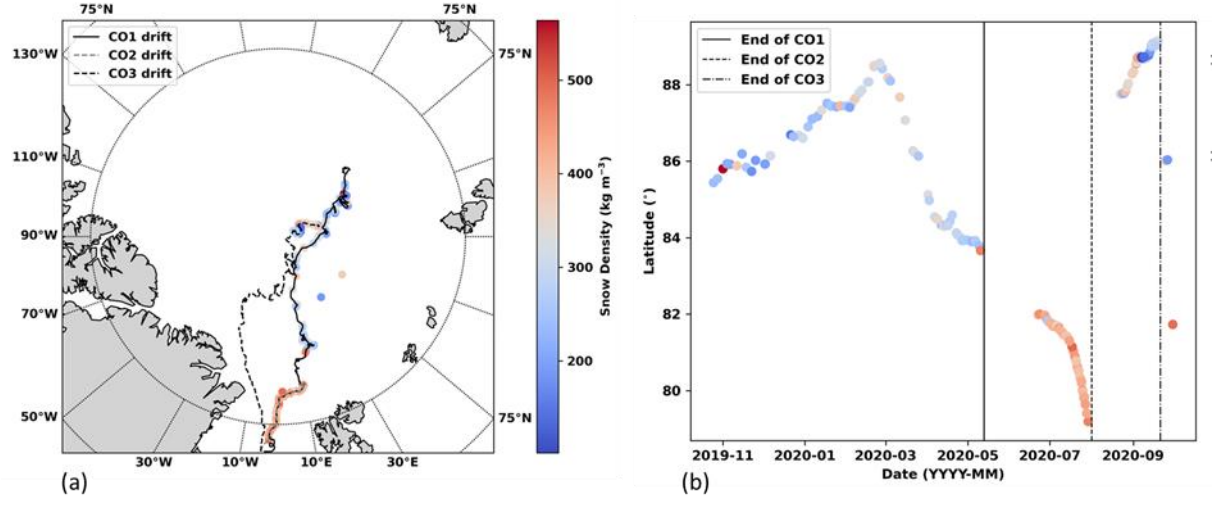

Figure 1: The MOSAiC ice camp drift trajectory. CO represents the central observatory camp (a) Snow density along the time and latitude of the observations, and (b) snow density along the drift. The colored dots represent the observed mean bulk snow density using cylinder snow samplers (Macfarlane et al., 2023a). The color bar illustrates the density values in a) and b).

https://doi.org/10.5194/egusphere-2025-1164
Preprint. Discussion started: 3 April 2025

2.1 Weather data

Meteorological parameters were measured at the Central Observatory Met City at approximately 500 m distance from RV *Polarstern* (Shupe et al., 2022). A 10-m-high weather mast was installed. We use 2-m air temperature and 10-m wind speed to investigate their impact on snow density since those are fundamental meteorological parameters affecting snow metamorphism (Sommerfeld and LaChapelle, 1970, Domine et al., 2007). For modelling, the relative humidity (calculated based on in-situ observed air temperature and dew-point temperature) as well as downward shortwave and longwave radiative fluxes were used. The radiative fluxes were measured by a pyranometer and a pyrgeometer (Cox et al. 2021). Precipitation is the major source of snow accumulation and one of the most important input variables for snow and ice modeling. Wagner et al. (2022) estimated a total snow precipitation between the end of October 2019 and the end of April 2020 of 98-114 mm, which is in a good agreement with the ERA5 reanalysis product.

2.2 Snow data

During MOSAiC, a comprehensive sea ice and snow observational program was set up (Nicolaus et al., 2022). Two traditional measurements were employed to measure snow density: classical box density cutters and cylinder snow samplers for snow water equivalent (SWE) measurement (Proksch et al., 2016; Macfarlane et al., 2023a). Snow pits were dug weekly at various locations on undeformed first-year ice, second-year ice, and places close to open leads and pressure ridges. At each site, multiple snow pits spaced about 1 m apart were dug. The MOSAiC ice floe became snow-free by late June - early July (Itkin and Liston, 2024) when the observations were interrupted due to logistic constraints. The snow-like surface scattering layer (SSL) observed over bare ice during the melting season was included among the snow observations. The details of the snow observations are presented by Macfarlane et al. (2021, 2023a). This study focuses on the temporal evolution of surface (top 3 cm) and bulk snow (entire snow layer) densities.

2.2.1 Surface snow density

The surface snow density (ρ_{sfc}) data were collected at each snow pit site using a density cutter box (100 cm^3). The ratio between the snow sample weight and the box volume yields snow density. In addition to recording density, the surface snow type at each sample was documented. During the measurement course, a variety of surface snow types, including new snow, rime, surface hoar, glazed snow, drifted snow, wet snow, visible dust, frost flowers, surface crust, SSL, jewel snow, and frozen snow were observed. Different type of snow exhibits distinct grain size and structure, moisture content, and hardness, leading to a unique density range. For example, fresh snow typically has a density of about 50-100 kg/m^3, whereas the density of settled or wet snow can exceed 500 kg/m^3 (Domine et al., 2007), and the density of SSL can be up to 700 kg/m^3 (MacFarlane et al., 2023). Combining these types of snow within the surface layer would introduce substantial variability of surface snow density (Fierz et al., 2009; Pielmeier and Schneebeli, 2003). Different measurement techniques may cause different biases and uncertainties depending on the snow type. For instance, using a snow density cutter on fresh snow may result in less accurate

https://doi.org/10.5194/egusphere-2025-1164
Preprint. Discussion started: 3 April 2025

measurements than its application on settled snow due to the difficulty in sampling the very soft and fragile structure of fresh snow (Domine et al., 2008). In total, 209 surface snow density samples were collected during legs 1-5, with the majority of samples taken from undeformed sea ice.

2.2.2 Bulk snow density

The bulk snow density (ρ_b) can be derived by integrating the measured densities of the various snow layers. However, downscaling high-resolution measurements to coarser resolutions may introduce measurement error (Essery et al., 2013). For simplicity, we derived the bulk snow density based on snow depth and SWE measurements. Snow depth h_s was measured manually at snow pit sites. SWE was measured using a cylindrical SWE sampler. We calculated the snow bulk density ρ_b using the equation $\rho_b = (\text{SWE} \times \rho_w)/h_s$, where ρ_w *is* the density of water, assumed as 1000 kg/m^3. The relationship between SWE (mm) and snow depth (m) for the entire MOSAiC period and the winter-spring period is illustrated in Fig. 2. The slopes of the regression lines represent the estimated temporal average snow densities: 348 kg/m^3 for the entire MOSAiC period and 308 kg/m^3 for the winter-spring period. These values can be used as constant snow density for climate modelling.

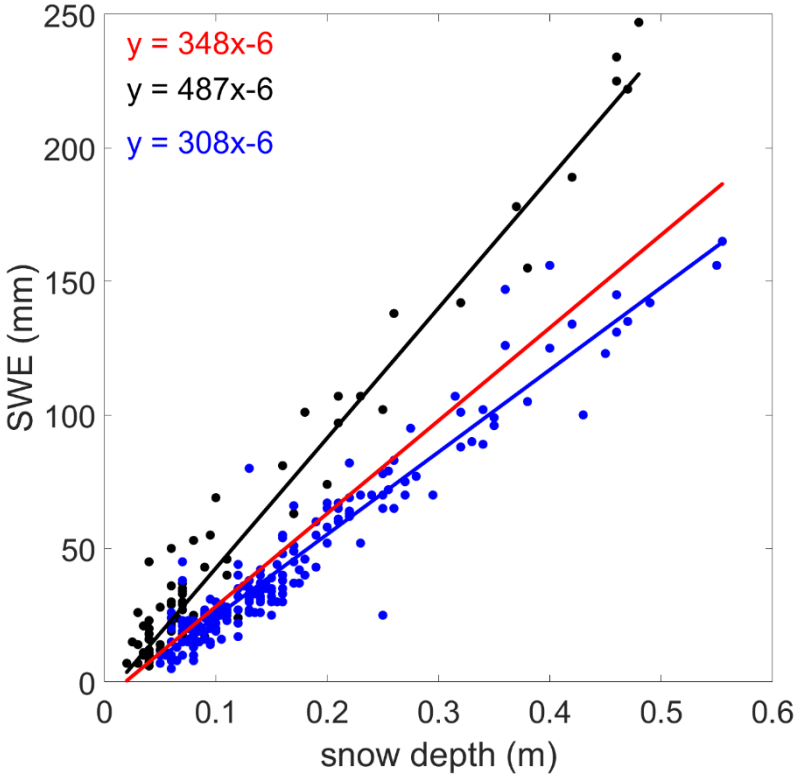

Figure 2: Scatterplot of SWE (mm) versus snow depth (m) from MOSAiC snow pit measurements over the entire MOSAiC period. Blue dots represent samples collected during the winter-spring period, while black dots denote samples from the summer-autumn

https://doi.org/10.5194/egusphere-2025-1164
Preprint. Discussion started: 3 April 2025

period. The slopes of the linear regression lines correspond to the bulk snow densities for the entire MOSAiC period (red), the winter-spring period (blue), and the summer-autumn period (black).

2.3 Snow density parameterizations

In climate models, snow density is either prescribed as a constant or parameterized as bulk values (McCreight and Small, 2014). The parameterization of bulk snow density is often derived based on a large set of in situ snow density observations using multiple empirical regression techniques involving a set of proxy variables, such as air temperature, wind speed, snow depth, and age of the snow cover (Pistocchi, 2016; Mizukami and Perica, 2008). In this study, we assess the three bulk snow density parameterization schemes by Sturm et al. (2010), Bruland et al. (2015) and Szeitz and Moore (2023) (Table 1). The E4 scheme by Anderson (1976) calculates snow density taking the effect of temperature on snow compaction into account by applying a prognostic equation. This scheme has been applied in sea ice modelling (Cheng et al., 2008, Wang et al., 2015). However, all schemes were developed based on terrestrial snow data sets.

Table 1: Bulk snow density parameterization schemes.

Sources	Snow density scheme
Sturm et al. (2010)	$\rho_b = \rho_0 + (\rho_m - \rho_0) \times [1 - \exp(-k_1 \times h_s - k_2 \times \mathrm{DOY})]$ (E1)
Parameters	$k_1 = 1.0 \times 10^{-3}$ and $k_2 = 3.8 \times 10^{-3}$ in this scheme are the fitting parameters, h_s (cm) is snow depth, DOY is day-of-year, ρ_0 (250 kg/m^3) and ρ_m (500 kg/m^3) are fitting parameters representing the initial and maximum bulk density.
Bruland et al. (2015)	$\rho_b = \rho_0 + (\rho_m - \rho_0) \times [1 - \exp(-k_1 \times h_s - k_2 \times z - k_3 \times T_d - k_4 \times V^*)]$ (E2)
Parameters	$k_1 = 5.03 \times 10^{-3}$, $k_2 = 1.8 \times 10^{-4}$, $k_3 = 4.77 \times 10^{-3}$, $k_4 = 4.2 \times 10^{-4}$; h_s (cm) is snow depth, z (m) is the elevation or the height above sea level of the location of the measurement; T_d (°C-days) is accumulated positive degree-day; V^* (m/s-days) is wind days when $T < 0$ ºC and wind speed $V > 2$ m/s.
Szeitz and Moore (2023)	$\rho_b = \rho_o + (\rho_m - \rho_0) \times (k_2 \times \mathrm{DOY}^2 - \exp(-k_1 \times h_s - k_3 \times T_d - k_4 \times T_{min} - k_5 \times P))$ （E3）
Parameters	$k_1 = 2.26 \times 10^{-1}$, $k_2 = 2.29 \times 10^{-5}$, $k_3 = 1.11 \times 10^{-2}$, $k_4 = 3.23 \times 10^{-4}$, $k_5 = 1.96 \times 10^{-2}$, h_s (cm) is snow depth; T_d (°C-days) is accumulated positive degree-day; T_{min} (°C) is minimum air temperature, P (mm) is daily total precipitation.

https://doi.org/10.5194/egusphere-2025-1164
Preprint. Discussion started: 3 April 2025

Anderson (1976)	$\frac{1}{\rho_b} \times \frac{\partial \rho_b}{\partial t} = C_1 \times \exp\left[-d \times \left(T_f - T\right)\right] \times W_S \times \exp(-C_2 \times \rho_b)$ (E4)
Parameters	T_f is the freezing temperature (273.15K); T is the air temperature(K); W_s (m) is total snow water equivalent; C_1= 5 $cm^{-1}hr^{-1}$; C_2 =21 $m^3\ Mg^{-1}$ and d=0.08K^{-1}.

2.4 Snow and ice model

A single column high-resolution thermodynamic snow and ice model (HIGHTSI) is used to simulate the impact of snow density on the thermal regime and mass balance of snow and ice. HIGHTSI computes the energy and mass balances at the snow surface, at the snow/ice interface, within the snow and ice layers, and at the ice bottom (Launiainen and Cheng, 1998). The snow-to-ice transformation is calculated in terms of ice mass balance. The refreezing of slush to snow ice due to ice surface flooding and the refreezing of melted snow to superimposed at the snow–ice interface is considered in the model (Cheng, et al., 2003). The penetration of solar radiation sometimes results in internal melting within the snow and ice (Zhao et al. 2022). The model can be used to track the thermal regime of snow and ice along ice drift trajectories (Cheng et al., 2008, 2021, Merkouriadi, et al., 2020). HIGHTSI uses time-dependent snow density (scheme E4) and snow heat conductivity (Sturm et al. 1997). The thermal properties (density, specific heat, and thermal conductivity) of sea ice are parameterized according to Yen (1981) and Pringle et al. (2007). In addition to this scheme, we incorporated into HIGHTSI the snow density schemes E1, E2, and E3 (Table 1) as well as the MOSAiC data-based prescribed snow density to investigate how the different snow density schemes affect the thermal regime of snow and sea ice. The meteorological parameters, including wind speed (V), air temperature (T_a), relative humidity (Rh), precipitation (P), as well as shortwave (Q_s) and longwave (Q_l) radiative fluxes from the ERA5 reanalysis along drift trajectory of MOSAiC CO (Leg 1-3) were used as forcing data for the HIGHTSI model (Fig. S1). The model parameters are based on in situ observations and literature values and are listed in Table S1. To compare the observations and model results, we pre-processed the time series of snow density and used a time-dependent snow density for each model run. This was derived either based on the 10-day moving average from in situ snow density observations or on the snow density parameterization schemes, outlined in Table 1.

3 Results

Quality control was applied to the snow density data. Based on prior observational data analyses (Sturm et al., 2002), snow density values exceeding 700 kg/m³ across the entire dataset, as well as those surpassing 500 kg/m³ from October to May, were excluded.

https://doi.org/10.5194/egusphere-2025-1164
Preprint. Discussion started: 3 April 2025

3.1 MOSAiC statistics of observed snow density

For the whole MOSAiC observation period, the observed surface snow density samples revealed a large variability, ranging from 82 to 498 kg/m³, with a mean and a standard deviation of 311 kg/m³ ± 94 kg/m^3. The bulk snow density samples varied from 83 to 690 kg/m³, with a mean and a standard deviation 291 ± 106 kg/m^3.

Figure 3 presents the frequency distribution of both bulk snow density and surface snow density for the entire MOSAiC observation period and for the winter-spring period (October to May). For the whole MOSAiC period, 272 snow bulk measurements obtained from SWE and snow depth observations and 209 snow density measurements of the top 3 cm layer collected using a cutter were available for reference. 197 snow bulk density measurements and 89 surface snow density measurements were collected during the winter-spring period. In the uppermost 3 cm layer, the snow density during the winter-spring period ranged from 82 to 432 kg/m³, with an average of 282 kg/m³, and the standard deviation was 77 kg/m³.

For the winter-spring period, the frequency distribution of surface snow density shows two main peaks around 250 and 300 kg/m³ (Fig. 3a). Fresh snow density may vary over a broad range, typically from 100 to 350 kg/m³ (Roebber et al., 2003). Both peaks fall within this range, suggesting that fresh snow is an important component of the surface snow distribution. However, the observed surface snow density may also be influenced by environmental factors such as wind compaction and temperature-induced snow metamorphosis. After snowfall, surface snow undergoes densification due to wind-induced compaction and temperature-driven metamorphism, During the freezing period, the wind exerts a strong effect on the surface snow layer, leading to the formation of wind slab snow (Seligman, 1936). Wind slab density typically varies from 350 kg/m³ to 500 kg/m³ (Derksen et al., 2014; Domine et al., 2007). The peak corresponding to the highest snow density (around 300 kg/m³) is below this range (Fig. 3a). This could be due to the effect of topography on the snowdrift accumulation patterns, which caused spatial heterogeneity in the densification process.

The distribution of surface snow density throughout the entire observation period (blue line in Fig. 3a) resembles that observed during the winter-spring period. However, the peaks are far less pronounced, and the distribution includes a much higher frequency of large snow densities, due to the dominant presence of SSL during the melting period. In fact, summer SSL observations cover approximately half of the surface snow density observations (Fig 4e). A similar double-peak surface snow density distribution was also observed in snow on the Greenland ice sheet (Fausto et al., 2018), supporting the hypothesis that the processes driving the density distribution (precipitation, topography, wind-induced snowdrift and snow packing) are not regionally confined but are common in cold, windy environments where snowfall events and wind-induced snow drift frequently occur.

The bulk snow density shows a right-skewed unimodal distribution, with the median snow density during MOSAiC around 250 kg/m³ (Fig. 3b). Most bulk snow density values are centered around 250 kg/m³, in line with the primary bulk snow density applied in typical snow schemes. Additionally, the snow depth and various metamorphic processes affect the bulk snow density, whose impact increases over time as the snowpack evolves.

https://doi.org/10.5194/egusphere-2025-1164
Preprint. Discussion started: 3 April 2025

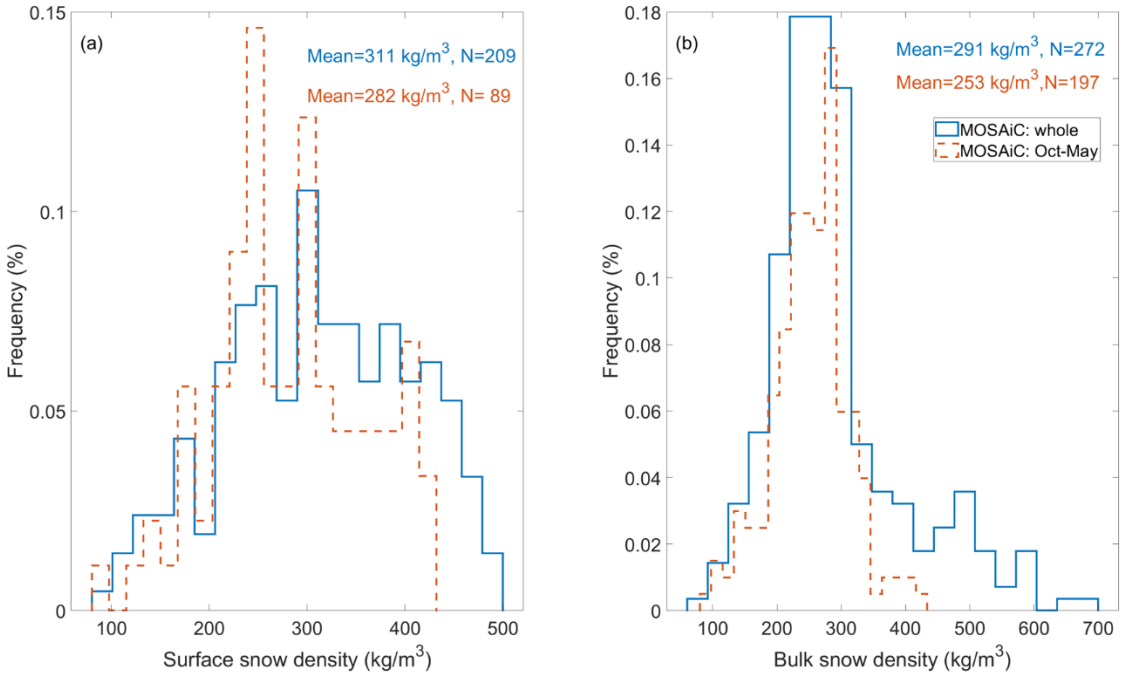

Figure 3: Frequency (%) distribution of surface snow density (a) and bulk snow density (b). The blue and orange colors represent the density distribution for the entire MOSAiC period and the winter-spring period, respectively. The mean snow density and sample numbers are provided in the plot. Density bins of 21 kg/m³ and 32 kg/m³ are used in (a) and (b), respectively.

3.2 Snow density evolution over the annual cycle

The time series of observed surface snow density (ρ_{sfc}), bulk snow density (ρ_b), air temperature, and wind speed, snow depth and sampling distribution are shown in Fig. 4. According to the annual cycle of air temperature, we can categorize four periods: The cold season (defined as Stage I) starts from the beginning of the observations and lasts until 18 February. During this period the mean air temperature is -25 °C. The freezing period (Stage II) starts from 19 February to 10 May. Within this period the air temperature increases from -40 °C to -10 °C. The melting period (Stage III) is from 13 June until the end of August with a mean air temperature of 0.1 °C. The cooling season (Stage IV) starts from 2 September and lasts until the end of the ice camp (20 September). During this period, the mean air temperature was -3.1 °C.

https://doi.org/10.5194/egusphere-2025-1164
Preprint. Discussion started: 3 April 2025

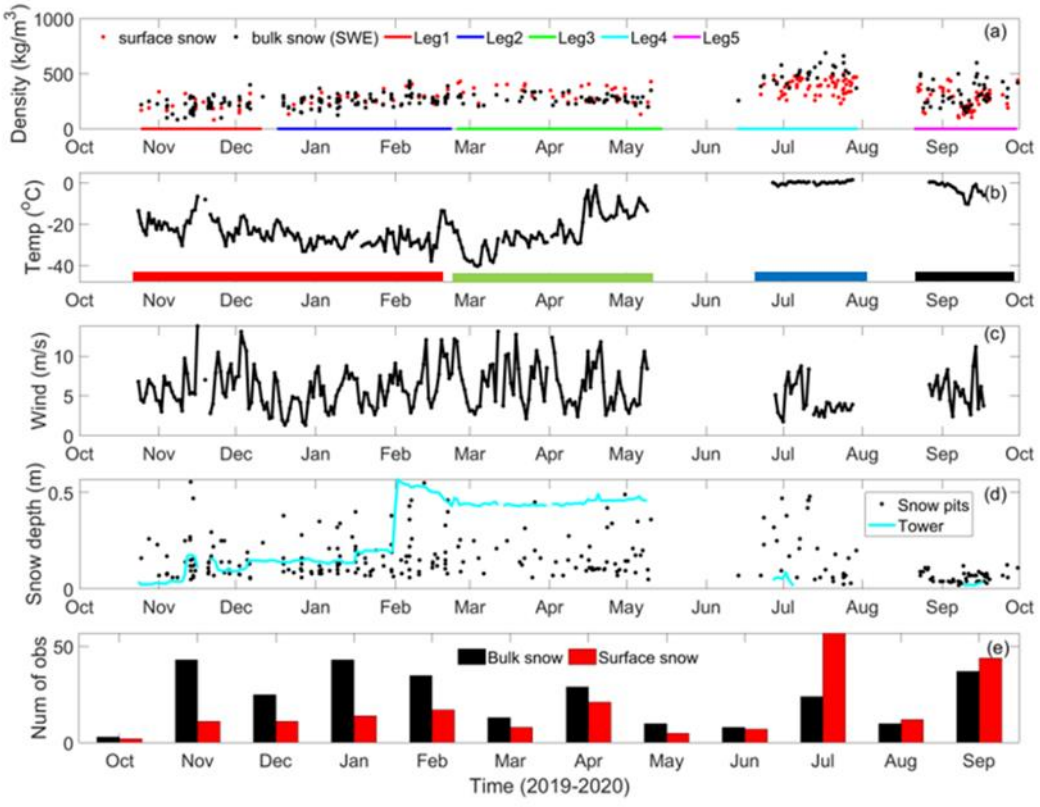

Figure 4: Time series of (a) observed snow density (kg/m³) for surface snow (red) and bulk snow (black), (b) observed air temperature (˚C) at 2 m height, and (c) wind speed (m/s) at 10 m height. The colored horizontal bars in (b) represent the four stages (red: I; green: II; blue: III; and black: IV). The bottom-colored bars in (c) refer to the MOSAiC legs 1 - 5. (d) Time series of snow depth: black dots represent observations from snow pits, and the light blue line indicates measurements from the weather tower. (e) Distribution of the number of observations for bulk snow (black bars) and surface snow (red bars).

During Stage I, both surface and bulk snow densities range between 150 and 400 kg/m³, with mean values of 252 kg/m³ for surface snow density and 247 kg/m³ for bulk snow density. In Stage II, the rise in air temperature affects the surface snow density, resulting in higher surface snow density compared to bulk density. Stage III is characterized by substantial ice melting. The preferential melting of ice crystal boundaries produces the SSL (Smith et al., 2022), a porous, snow-like layer where the density increases with depth (Macfarlane et al., 2023b). The SSL is less dense than the sea ice from which it is generated, but it is much denser than snow. The meltwater drains to melt ponds and leads, leaving the SSL relatively dry. As the top SSL layer melts, there is a simultaneous transformation of the underlying bare ice to the SSL. Thus, the thickness of the SSL remains stable throughout the summer (Macfarlane et al., 2023b). During Stage IV, air temperatures drop below 0°C. This phase is marked by the refreezing of melt ponds and the onset of new snowfall, signalizing the beginning of a winter season. The snowpack/SSL undergoes significant restructuring as it transitions from a melting phase to a refreezing one, laying the foundation for the subsequent accumulation period. The average wind speed during the study period was 5.9 m/s, with the highest and lowest wind speeds recorded at 13.8 m/s and 1.3 m/s, respectively. The snow depth exhibited significant

https://doi.org/10.5194/egusphere-2025-1164
Preprint. Discussion started: 3 April 2025

temporospatial variations and localized features (based on tower measurements). The mean snow depth observed during MOSAiC was 0.16 m, with the thickest and thinnest snow depths measuring 0.49 m and 0.05 m, respectively. Snow sampling during the MOSAiC expedition was not evenly distributed in time (Fig. 4e, Fig. S2) due to logistical challenges (Itkin et al., 2024). This impacted the snow depth and density distributions, which does not include the end of the snow melting stage and represents some snow stages (such as SSL in July-September) more than others.

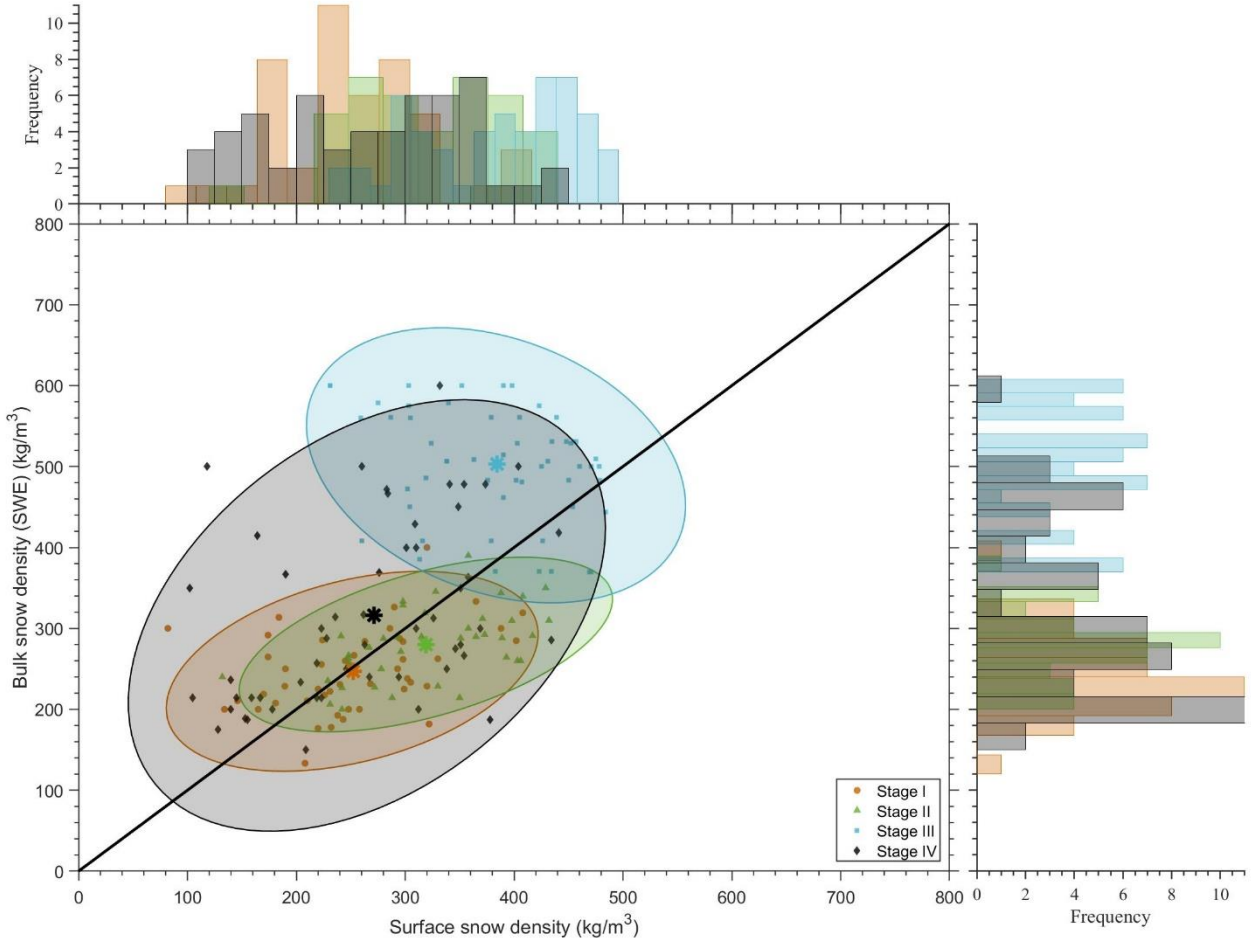

Figure 5: Simultaneous surface and bulk snow densities extracted from data samples (Fig. 4) during the four stages. The asterisks indicate the mean snow densities (Stage I: ρ_{sfc} =252 kg/m^3, ρ_b = 247 kg/m^3; Stage II: ρ_{sfc} =319 kg/m^3, ρ_b = 280 kg/m^3; Stage III: ρ_{sfc} =384 kg/m^3, ρ_b = 503 kg/m^3, and Stage IV: ρ_{sfc} =271 kg/m^3, ρ_b = 316 kg/m^3). The ellipse shadings represent bivariate Gaussian ellipses in terms of the 95% confidence intervals for each stage. Bar plots on the top and right side depict the absolute frequency (counts) of the observed surface snow density and bulk snow density.

Figure 5 illustrates the relationship between bulk snow density and surface snow density across four temperature-based stages (I-IV). The bulk and surface snow density samples are collected simultaneously for comparsion. The scatter plot displays stage-specific distributions, with ellipses representing correlation patterns. Marginal histograms provide the corresponding

https://doi.org/10.5194/egusphere-2025-1164
Preprint. Discussion started: 3 April 2025

245 frequency distributions. In Stage I and Stage II, a positive relationship exists between bulk and surface snow densities. The ellipse for Stage II is the most flattened, indicating the strongest correlation, whereas Stage I exhibits a weaker correlation with a less flattened ellipse. The slope of the major axis is less than 1, suggesting that surface snow density varies more than bulk density. Frequency distributions reveal that bulk snow density is more concentrated, indicating greater uniformity in deeper snow layers. In Stage IV, the ellipse is more circular, and the slope exceeds 1, indicating that bulk snow density varies more
250 than surface snow density. The frequency distribution shows a broader spread in bulk density, reflecting greater heterogeneity within the snowpack as internal processes dominate. Stage III demonstrates the weakest correlation, with a nearly circular ellipse and a negative slope, indicating the more independent relationship between bulk and surface densities. This weak relationship suggests that different processes are influencing the surface and bulk snow densities at this stage.

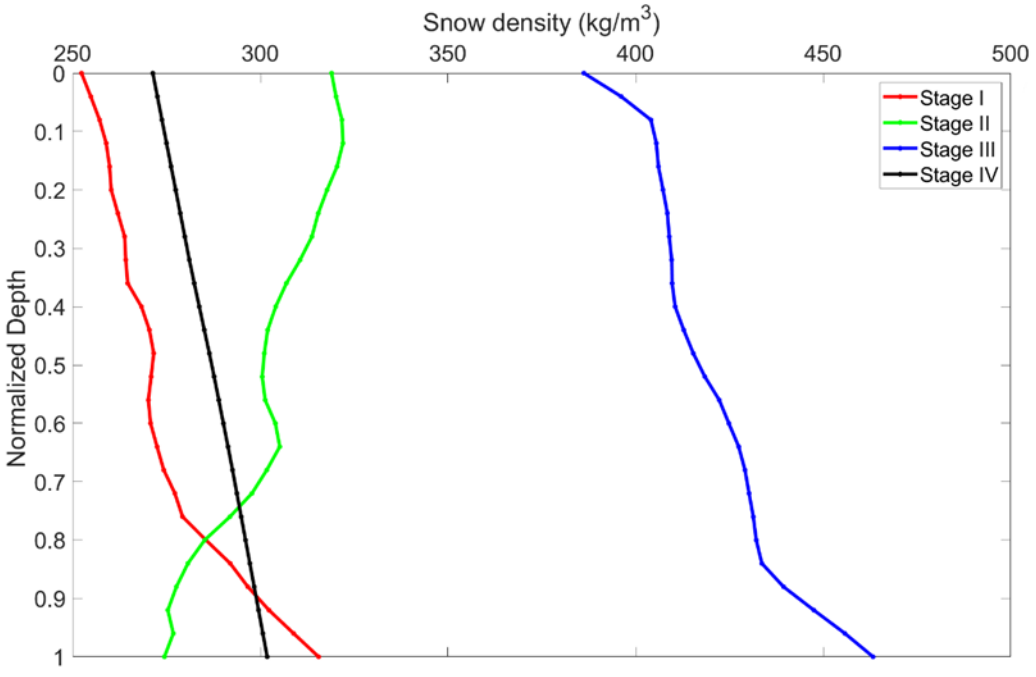

255 **Figure 6: Normalized mean snow density profiles during each stage. The mean snow depths were 0.15 m, 0.18 m, 0.15 m, and 0.06 in Stage I, II, II and IV, respectively.**

The normalized mean vertical profile of snow density is shown in Fig. 6. The measurements were obtained using a snow cutter. Normalization was necessary because the snow depths at each snow pit differed from one another. During Stage I, the mean snow density gradually increases with depth, rising from 265 kg/m³ at the surface to 310 kg/m³ at the bottom. This is probably
260 because at the bottom of the snowpack, the high-density SSL, formed during the melting, remains buried under the new snow during the freeze-up. The snow layers right above the SSL deposited in autumn, in temperature regimes that were warmer than in late winter and, thus, favored denser, more metamorphosed snow compared to the overlying snow layers. During Stage II, the density distribution reversed compared to Stage I. The snow density gradually decreases with depth, from 310 kg/m^3 at the

https://doi.org/10.5194/egusphere-2025-1164
Preprint. Discussion started: 3 April 2025

surface layer to 270 kg/m^3 at the snow/ice interface. The increase in surface snow density during Stage II can be attributed to wind compaction (Leeuw et al., 2023), while the decrease in snow density at the snow/ice interface resulted from the metamorphism of the SSL crystals into larger and looser depth hoar crystals (King et al., 2020). At the end of April, episodic surface melting occurred in association to warm-air intrusions (Fig. 4b), and the refreezing of percolated meltwater explains the density maxima below the surface layer and at an intermediate depth layer. It is evident that the SSL during the ice melting Stage III is denser than the snow present in the other stages. The SSL density is highest at the ice-SSL interface, where new SSL forms by disaggregation of the sea-ice structure due to melting, and is lowest at the surface, where the SSL melting is more pronounced. During the sea-ice refreezing in Stage IV, the density profile includes the SSL at the bottom and successively accumulated snow layers on the top. Hence, the density profile shows a linear increase with depth, similar to the vertical profile in Stage I. As a result, the observed snow density at each vertical level exhibits distinct spatial variability (Fig. S3).

For the whole MOSAiC expedition, surface snow/SSL density varied between 82 and 498 kg/m^3, while the snow/SSL density at the bottom of the snowpack exhibited an even broader range, from 102 to 690 kg/m^3. The fluctuations were larger at the bottom, because the dataset includes the highly dense SSL samples of the early stage of the ice-to-snow transformation process occurring close to the ice-SSL interface.

3.3 Impact of wind on snow density

Wind can impact snow density via different mechanisms. On one hand, wind can compact the snowpack, which results in a higher snow density; on the other hand, strong enough wind results in drifting or blowing snow, generating large spatial variations in snow depth, which also impact snow density. Linear regressions were calculated to quantify the wind compaction of snow. The cumulative wind speed is the sum of daily mean wind speeds (in m/s) over a cumulative number of days, analogously to temperature in degree-days. Particular attention was paid to the sensitivity of the regression coefficients to the accumulation time window.

https://doi.org/10.5194/egusphere-2025-1164
Preprint. Discussion started: 3 April 2025

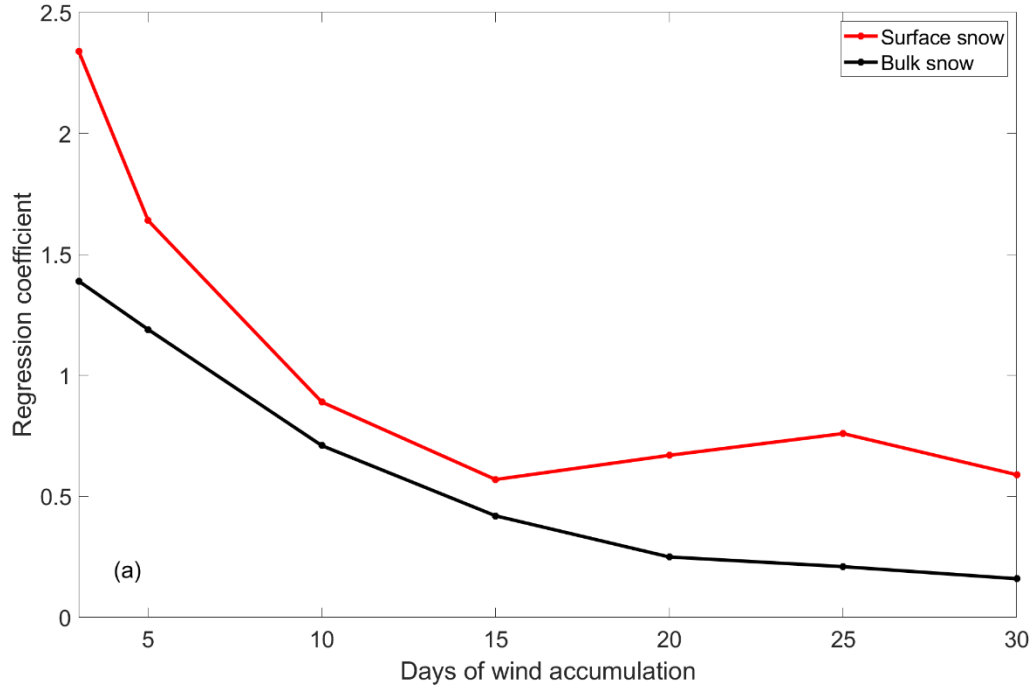

285

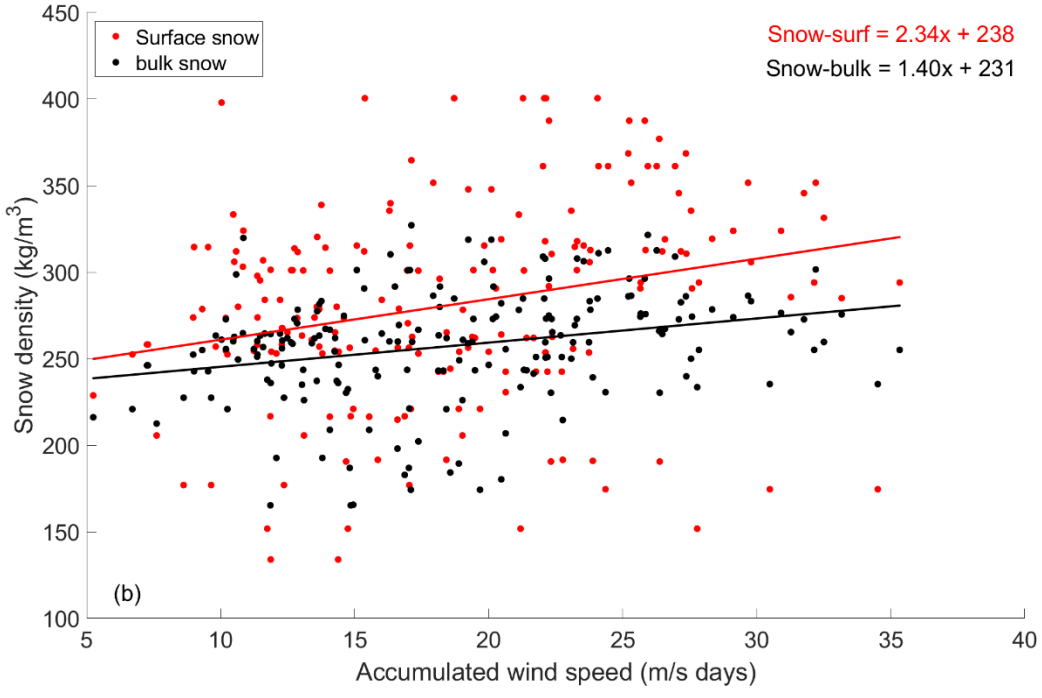

https://doi.org/10.5194/egusphere-2025-1164
Preprint. Discussion started: 3 April 2025

Figure 7: (a) Regression coefficients for the dependence of surface (red) and bulk (black) snow density on accumulated wind speed, with accumulation time windows ranging from 3 to 30 days. All regression coefficients are statistically significant at the 95% confidence level. (b) Dependence of surface and bulk snow density on accumulated wind speed during the previous 3 days, with coefficients statistically significant at the 99% confidence level.

The regression coefficient for surface snow density decreased from 2.34 at a 3-day accumulation period to 0.59 at a 30-day period (Fig. 7a). The shape of the curves in Fig. 7a indicates that the sensitivity of surface snow density to cumulative wind speed is highest over shorter periods (an example is shown for 3-days in Fig. 7b) but declines rapidly as the accumulation period increases. For bulk snow density, the coefficients were consistently smaller than for the surface snow density, ranging from 1.39 for a 3-day accumulation period to 0.16 for 30-days period (Fig. 7a). This is as expected, as the air-snow momentum flux can most efficiently deform the snow crystals at the surface of the snowpack. The decrease of the coefficients with increasing accumulation time may be interpreted as follows: after a snowfall event, the wind can initially induce strong deformation of the snow crystals. However, once the weakest crystal structures are broken, the rate of deformation slows down. Also, over increasing accumulation periods, other environmental and snowpack processes may start to dominate the wind's influence. For shorter periods (within one month), all the regression coefficients for the surface and bulk snow densities are statistically significant at the 95% confidence level. In the case of surface snow density, the regression coefficients level out approximately at a 15-day accumulation period (Fig. 7a).

3.4 Evaluation of snow density parameterizations

The analyzed snow density characteristics were used to evaluate four different parameterization schemes (see Section 2.3; Table 1). We focus on data from legs 1-3 (October-May) when the meteorological parameters were observed along a continuous ice drift trajectory. As already mentioned, the observed snow density shows a high variability throughout the season, ranging from under 100 kg/m³ up to close to 500 kg/m³ (Fig. 4), which can be attributed to both the snow densification processes and differences in the spatial distribution.

Snow density scheme E1, which considers both snow depth and the number of winter days (DOY) as influencing factors, shows a gradual increase in snow density over time (Fig. 8). The simulated values agree with the observed densities in the lower to mid-range. However, scheme E1 struggles to represent the response of density to large changes in snow depth. For instance, the effects of heavy snowfall events in November and February (visible in Fig. 4d) by short-term rapid increases in snow depth), as seen in the observed bulk density changes (Fig. 4a and 8), are not reflected in the E1 parameterization. Consequently, E1 produces overly smooth snow density evolution, missing the pronounced effects of snowfall events.

In comparison, scheme E2, which considers the effects of snow depth, positive degree days, and wind speed days, reproduces density changes in response to snow depth changes in November and February. However, E2 consistently overestimates the bulk snow density relative to the observations.

Scheme E3, which depends on snow depth, temperature, accumulated positive degree-days, minimum air temperature, and precipitation, accounts for both mechanical and thermodynamic processes that influence snow structure and density. However, in November, E3 shows an excessively strong increase in snow density compared to the observations, and it simulates a too

https://doi.org/10.5194/egusphere-2025-1164
Preprint. Discussion started: 3 April 2025

slow increase of snow density until March. This indicates that, in E3, snow depth plays a crucial role in controlling snow density early in the season, but other factors, such as the duration of winter, may become more influential later in the season.

The snow density scheme E4 is the most complex one out of the four schemes evaluated here, and it is widely used in the sea ice research community (e.g., Essery et al., 2013). The scheme uses a prognostic equation that considers factors such as compaction due to overlying snow layers and metamorphic processes driven by temperature gradients. The initial snow density needs to be specified depending on the application. Here we select three categories of initial snow density to represent fresh new snow (150 kg/m³), intermediate snow (250 kg/m³) and average snow on Arctic sea ice (320 kg/m³) (King et al., 2020). The E4 simulations highlight the strong impact of initial snow density on snowpack evolution, especially early in the season. The lowest initial snow density results in the lowest predicted snow density throughout the season and provides a lower-bound estimate for snow density. It agrees with the observed lower values of density, especially early in Stage I. The intermediate initial condition gives a moderate estimate of snow density, generally following the observed evolution, but staying below the highest observed density values. Those can only be simulated with the highest initial density values. Although there is an obvious difference between the three different initial snow densities (range of 170 kg/m^3), the final difference in density at the end of the winter is relatively small (in the order of 15 to 20 kg/m^3).

All parameterization schemes reproduce the observed increase of the bulk snow density over the winter, but none of them match the observed data throughout the season. In particular, all schemes fail in reproducing the observed decrease of the snow density in April and May.

https://doi.org/10.5194/egusphere-2025-1164
Preprint. Discussion started: 3 April 2025

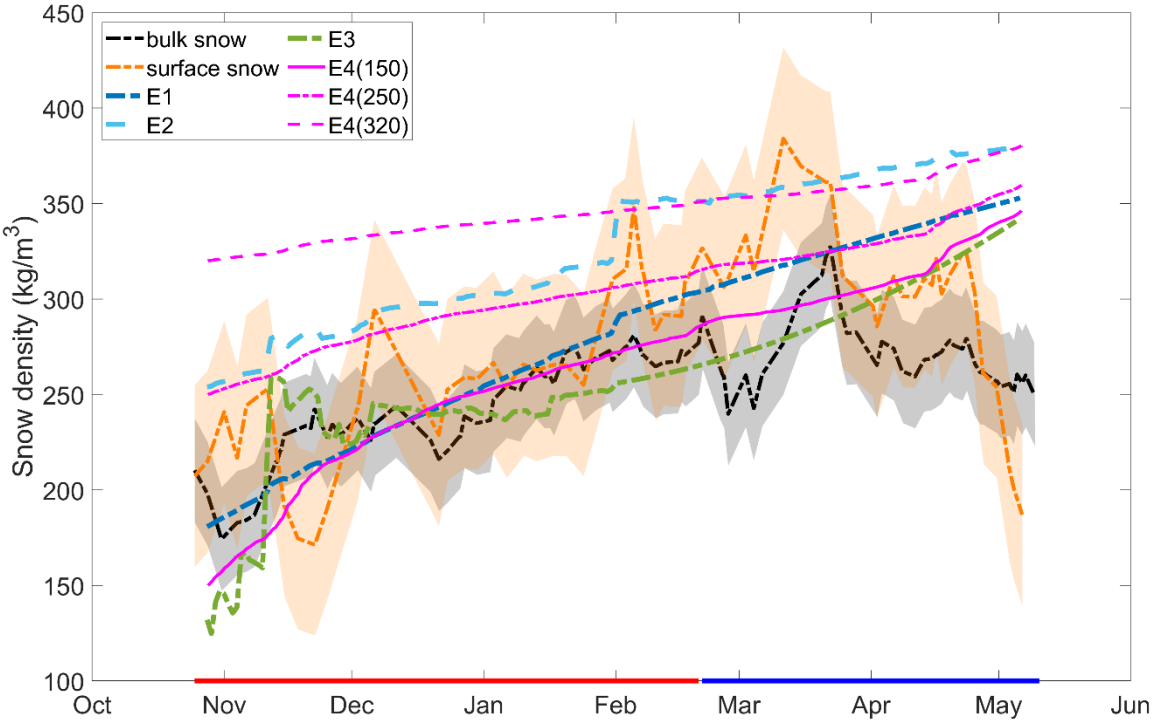

Figure 8: Temporal evolution of 10-day moving average bulk (black) and surface (orange) snow densities, along with their standard deviations (dark and light shaded areas for bulk and surface densities, respectively), as well as the time series of four snow density parameterization schemes E1-E4 (colored lines). E4 (magenta lines) was initialized with three different densities (150 kg/m³, 250 kg/m³, and 320 kg/m³). All simulations are for the winter-spring period (from October to May), covering stages I (red line at the bottom) and II (blue line at the bottom).

Table 2: Root-mean-squared error (RMSE), mean absolute error (MAE), and mean bias between observed and parameterized (E1-E4) daily mean bulk snow density.

	Daily mean bulk snow density (kg/m³)					
	E1	E2	E3	E4 (150)	E4 (250)	E4 (320)
RMSE	39	75	31	33	55	96
MAE	29	72	25	24	51	94
Mean bias	22	72	9	9	51	93

The root-mean-squared error (RMSE), mean absolute error (MAE), and mean bias of the parameterized daily mean snow densities are presented in Table 2. All parameterizations (E1-E4) have a positive mean bias of calculated bulk snow density compared to the observations. E2 and E4(320) exhibit the largest RMSE and MAE compared with the observations. E1 and E3 show lower RMSE and MAE, suggesting improved performance in capturing the observed snow density evolution

https://doi.org/10.5194/egusphere-2025-1164
Preprint. Discussion started: 3 April 2025

compared to E2. It is important to note that the comparison with observations is based on the daily mean bulk snow density, which may obscure some of the dynamic aspects of the snow density evolution, such as the spatially heterogeneous snow compaction and redistribution driven by the interaction between wind and surface roughness. Daily averaging may reduce the short-term variability in snow density data and diminish the ability to capture short-term changes and localized events within the snowpack. The results of the E4 scheme highlight the importance of the snowpack conditions at the beginning of the season. The initial snow density significantly influences the evolution of the snowpack. The lowest RMSE and MAE are obtained with an initial snow density of 150 kg/m³. None of the snow density schemes can capture the short-term temporal variability of the observed snow density.

3.5 Model experiments

3.5.1 Impact of snow density on sea ice

Here, we incorporate a time series of MOSAiC surface (ρ_{sfc}) and bulk (ρ_b) snow density, along with snow density schemes (E1–E4), into the HIGHTSI model to investigate how the selection of snow density scheme affects the thermal regime of snow and sea ice (refers as modelling group 1). The time series of ρ_{sfc} and ρ_b are presented as 10-day moving averages with temporal standard deviations (Fig. 8). For E1-E3 simulations, we applied the initial snow density of 250 kg/m^3. The E4 simulations, which use specified initial snow densities (as described in the previous section), are labeled as E4(150), E4(250), and E4(320), respectively. The modeled mean temperatures of the snow surface (Tsfc), snow layer (Tsnow), and ice layer (Tice), as well as the mean ice thickness (Hice) during the simulation period (from 1 October 2019 to 31 May 2020), are presented in relation to the mean snow density (Ds) used in each modeling experiment (Table 3). For comparison, we performed another group of model experiments (refers as modelling group 2) using constant snow density values of 180, 200, 220, 250, 270, 300, and 320 kg/m^3.

The mean ρ_{sfc} is 24 kg/m^3 larger than ρ_b. The mean standard deviations of ρ_{sfc} and ρ_b are 47 kg/m^3 and 28 kg/m^3, respectively. The mean bulk snow density (ρ_b) of the E1-E4 simulations is 294 kg/m^3 with a standard deviation of 41 kg/m^3. The Ds values calculated applying E1, E3, E4(150) and E4(250) fall within the ρ_{sfc} observation range [231-325 kg/m^3], with the E1 yielding the closest match to the observed mean ρ_{sfc} (279 vs. 278 kg/m^3). On the other hand, the Ds calculated applying E1, E3, and E4(150) fall within the ρ_b observation range [226-282 kg/m^3], with the E4(150) scheme yielding the closest match to the observed mean ρ_b (265 vs. 254 kg/m^3).

Table 3: The mean snow density (Ds) and modeled mean values of surface temperature (Tsfc), snow temperature (Tsnow), ice temperature (Tice), and ice thickness (Hice) using the 10-day moving average of observed surface (ρ_{sfc}) and bulk (ρ_b) snow density, as well as snow density schemes E1–E4 with different initial snow densities. All values represent averages for the period from October to May. The ± values indicate the results incorporating the standard deviations of ρ_{sfc} and ρ_b, respectively.

Mean values during simulation period	ρ_{sfc}	ρ_b	E1	E2	E3	E4 (with different initial snow density kg/m^3)		
	10-day moving average		ρ_0 = 250 kg/m^3			E4(150)	E4(250)	E4(320)

https://doi.org/10.5194/egusphere-2025-1164
Preprint. Discussion started: 3 April 2025

Ds (kg/m^3)	278 ± 47	254 ± 28	279	329	239	265	305	347
Tsfc (°C)	-24.6±0.03	-24.6 ±0.03	-24.8	-24.7	-24.9	-24.6	-24.6	-24.5
Tsnow (°C)	-18.0± 0.4	-17.8 ± 0.3	-16.6	-17.2	-16.1	-17.8	-18.2	-18.6
Tice (°C)	-7.3± 0.4	-7.0 ± 0.2	-5.9	-6.5	-5.5	-7.1	-7.4	-7.8
Hice (m)	1.08 ± 0.4	1.05 ± 0.03	0.87	0.97	0.80	1.06	1.10	1.16

In response to the Ds range of 226–347 kg/m³, the modeled mean surface temperature fluctuated by 0.4°C, showing a weak dependence on the applied snow density scheme (Fig. 9a). The corresponding Tsnow and Tice exhibited ranges of approximately 2.5°C and 2.3°C, respectively, showing a stronger response to snow density compared to the snow surface temperature (note the different vertical axes in Fig. 9a, b, and c). The modeled mean ice thickness (Hice) was 1.01 ± 0.12 m, with a variation range of 0.36 m. Different snow density schemes resulted in variations in the modeled ice thickness, with a standard deviation of 0.12 m, representing approximately 12% of the modeled mean ice thickness.

Linearity of Tsfc, Tsnow, Tice, and Hice with mean Ds is observed in two clusters of model experiments and observations (one cluster including E1, E2 and E3, and another cluster including mean ρ_{sfc}, mean ρ_b, and three E4s). The linearity indicates that the modeled Hice increases with increasing snow density, while the modeled Tsnow and Tice decrease with increasing snow density. A higher snow density results in higher thermal conductivity and volumetric heat capacity, enhancing the conductive heat flux and allowing more heat to be transferred toward the snow surface. This enhanced heat transfer, associated with higher snow density, also accounts for the thicker ice and slightly warmer surface temperature. It is noteworthy that the differences in the modeled Tsfc, Tsnow, Tice, and Hice may be attributed not merely to the differences in snow density alone, but also to other parameters associated with snow density, such as thermal conductivity and volumetric heat capacity. This is because HIGHTSI applies time-dependent snow thermal conductivity, parameterized as a function of snow density (Sturm et al., 1997). This may explain why the Ds values of the time series for ρsfc and E1 are nearly identical, while the calculated snow and ice variables differ (Table 3). When a constant snow density is applied in HIGHTSI, the linear relationship between snow density and the thermodynamic state of snow and ice becomes more pronounced and aligns with the snow density cluster (E1–E3) in modeling group 1. Tsfc and Hice increase linearly by 0.27°C and 0.23 m, respectively, while Tsnow and Tice decrease linearly by 1.48°C and 1.34°C, respectively, in response to an increase in snow density from 180 to 320 kg/m³ (“+” connected lines in Fig. 9).

https://doi.org/10.5194/egusphere-2025-1164
Preprint. Discussion started: 3 April 2025

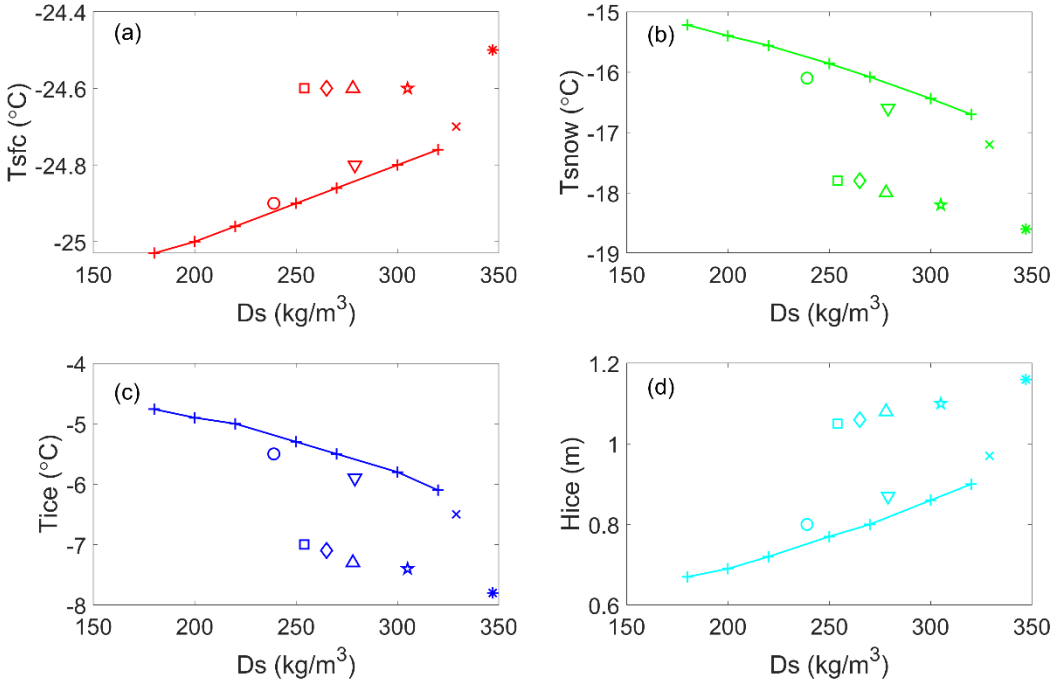

Figure 9: Modelled (a) mean snow surface temperature (Tsfc), (b) averaged in-snow (Tsnow) and (c) in-ice (Tice) temperatures and (d) mean ice thickness (Hice) as a function of the mean snow density (Ds). The symbols presented in the picture represent results of modelling group1 using different snow density schemes (E3:○, ρ_b:□, E4(150):◊, ρ_{sfc}:Δ, E1:∇, E4(250):☆, E2:× and E4(320):∗). The "+" connected lines represent values obtained from modelling group 2 experiments applying constant snow density values of 180, 200, 220, 250, 270, 300, and 320 kg/m^3.

3.5.2 Impact of precipitation on sea ice

During the MOSAiC expedition (October-May), the measured snow water equivalent (SWE) showed large spatiotemporal differences (Matrosov et al., 2022). SWE measurements are a major proxy for snow accumulation in winter and spring and for ice-to-SSL transformation in summer. Winter and spring snow accumulation depends on precipitation and wind-forced snow redistribution. We made model sensitivity experiments to understand the impact of precipitation and wind-induced snow redistribution on snow and ice thermodynamic parameters in the winter-spring MOSAiC period applying the measured SWE in each month of the MOSAiC expedition from October to May. The SWE was measured by different types of sensors (see Matrosov et al., 2022; their Table 1). We used a constant snow density (330 kg/m^3) to convert SWE to snow accumulation. This criterion was applied in previous studies (e.g., Huwald, et al., 2005). The bulk snow density ρ_b was determined by applying observed 10-day moving average (black dash line in Fig. 8). The model experiments were carried out in the same manner as in the case of snow density (ERA5 weather forcing, same model parameters, except that the observed SWE using different sensors were used as source for snow accumulation). The results are presented in Fig. 10.

https://doi.org/10.5194/egusphere-2025-1164
Preprint. Discussion started: 3 April 2025

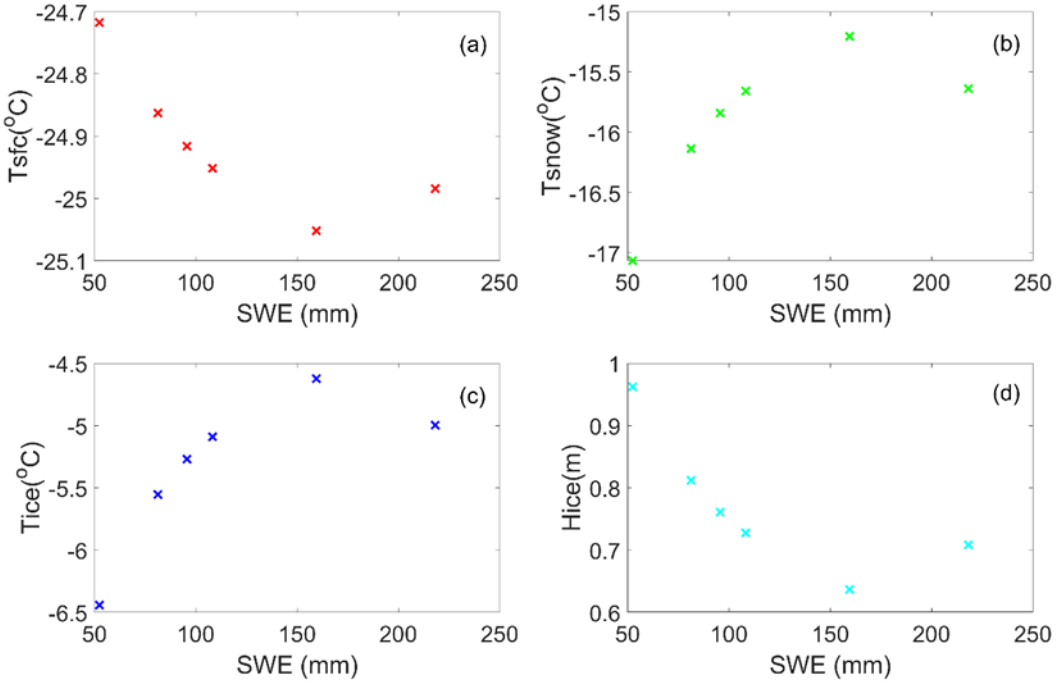

Figure 10: Modelled (a) mean snow surface temperature (Tsfc), (b) averaged in-snow (Tsnow) and (c) in-ice (Tice) temperatures and (d) mean ice thickness (Hice) as a function of SWE (proxy for snow accumulation resulting from precipitation and wind-induced snow redistribution) for October-May.

Table 4: Modelled mean snow and ice thermodynamic parameters using observed SWE as model input for snow accumulation. P1-P6 refers to the total snow accumulation observed by different sensors (Matrosov et al., 2022).

	Run P1	Run P2	Run P3	Run P4	Run P5	Run P6
SWE (mm)	96	81	160	218	53	108
Tsfc (°C)	-24.9	-24.9	-25.1	-24.9	-24.7	-24.9
Tsnow (°C)	-15.8	-16.1	-15.2	-15.6	-17.1	-15.7
Tice(°C)	-5.3	-5.6	-4.6	-5.0	-6.4	-5.1
Hsnow (m)	0.30	0.25	0.43	0.54	0.16	0.34
Hice(m)	0.76	0.81	0.64	0.71	0.96	0.73

The modeled surface temperature is not sensitive to the uncertainty in total snow accumulation as shown by the small standard deviation (0.14 °C) between the mean temperatures obtained applying different sensors (Table 4). The standard deviation among the modeled mean in-snow and in-ice temperatures (0.8 °C and 0.7 °C, respectively) reveals that the modelled temperature response to uncertainties in SWE (snow accumulation) is similar to the modelled temperature response to the uncertainty in parameterized snow density (Table 3). The modelled Tsnow and Tice vary over a range of 2.1 °C each when

https://doi.org/10.5194/egusphere-2025-1164
Preprint. Discussion started: 3 April 2025

changing SWE (snow accumulation) forcing, similar to the Tsnow and Tice variations with respect to different snow density parameterizations. Also, the model sensitivity of Hice to the applied SWE/snow accumulation (seen as a 0.13 m standard deviation of the means, Table 4) was similar to the sensitivity of Hice to the applied snow density parameterizations (Table 3). The modelled snow and ice temperatures as well as the snow and ice thicknesses show a nonlinear relationship to SWE during the modelling period. More snow accumulation leads to a thicker snowpack and a stronger insulation effect. As a result, the in-snow and in-ice temperatures increase, resulting in thinner ice. However, a major further increase in snow accumulation would reverse the above processes due to snow-to-ice transformation via surface flooding and resulting snow-ice formation (Saloranta, 2000). The response of the modelled parameters (Fig. 10) to increased SWE are opposite to their response to increased snow density.

4 Discussion and conclusion

The mean surface and bulk snow densities are comparable during stages I, II and IV, as the bulk snow density primarily reflects the cumulative effect of overlapping surface snow layers. However, during the melting season (III), the bulk snow density exceeds the surface snow density by 119 kg/m3. This discrepancy arises from processes characteristic of the melt period: intense surface melting and the downward percolation of meltwater reduce near-surface snow density, while the refreezing of meltwater at deeper layers increases density at those depths (Pirazzini et al., 2006; Vihma et al., 2011). In these deeper layers, density increases almost monotonically from the surface to the bottom. These findings underscore the significant influence of seasonal melting and refreezing processes on the vertical density structure of snow.

In winter, wind contributes to the spatial snow depth and density heterogeneity through the interaction with the surface topography. At the MOSAiC Central Observatory, Itkin et al. (2023) demonstrated that the interaction of wind, drifting snow, and sea ice roughness explains up to 85% of the observed snow depth variability over both level and deformed ice. In the Canadian Arctic, Iacozza and Barber (1999) observed that the wind direction during depositional storm events impacts the distribution of snow dunes. In summer, as snow melts over the Arctic sea ice, a SSL develops during the melting process. This layer forms as a highly porous surface crust on the melting sea ice, resulting in a density that is greater than that of snow but lower than that of sea ice (Macfarlane et al., 2023c). During autumn, winter, and spring, rain-on-snow (ROS) events can lead to the formation of a hard ice crust layer on the snow surface (Rennert et al., 2009). During the MOSAiC campaign, few ROS events were observed, which triggered surface melting in April (Svensson et al., 2023) and September (Stroeve et al., 2022). This resulted in the densification of the snowpack (Stroeve et al., 2022).

During winter-spring, the MOSAiC surface snow/SSL density shows two main peaks. The one at lowest density likely resulted from occurrences of fresh snow and snowdrift accumulation on the leeward side of topographic protrusions. The one at highest density is probably associated with snow densification induced by wind compression on the windward side of topographic protrusions, and to snow metamorphism driven by the energy and moisture exchange with the atmosphere. The distribution of surface snow density during the entire MOSAiC period is less peaked and show a larger fraction of dense snow due to the

https://doi.org/10.5194/egusphere-2025-1164
Preprint. Discussion started: 3 April 2025

contribution of the summer SSL. A right-skewed unimodal distribution of the bulk snow density reflects the cumulative effect of multiple snow layers, influenced by surface deposition as well as by compaction, metamorphosis, and densification processes. The initial snow depth prior MOSAiC CO camp is important and has a significant role on the snow density distribution. Although there was heavy precipitation recorded in November and February (Matrosov et al., 2022), the cumulative seasonal snow accumulation was not large. Based on Koo et al., (2021), in the MOSAiC Central Distributed Network (DN) domain scale of about 50 km, the average initial snow depth was 16 cm. By the end of May, the net snow depth increased by approximately 5 cm, resulting in a ratio of snow depth accumulation to initial snow depth of about 0.3.

The mean vertical profile of snow density exhibited distinct patterns at each stage. At different depths, the spatial variation of snow density is also large among sample sites. From a snow climatology perspective, snow accumulation and melting cycles play critical roles in shaping snow density profiles (Warren et al., 1999). Sea ice topography influences snow depth distribution, which can lead to heterogeneous snow density structures (Iacozza and Barber, 1999). Regional and temporal variations in snow depth are governed by the complex interplay between atmospheric forcing, sea ice dynamics, and snow accumulation processes (King et al., 2020; Itkin et al., 2023). Integrating these factors determines the evolution of snow density.

Temporal variations in snow density were more pronounced than vertical variations. Both surface and bulk snow densities exhibited a non-monotonic increase during the winter and a decrease by the end of spring. The increase in snow density during winter aligns with Arctic snow climatology (Warren et al., 1999). However, the decrease in snow density during the melting in May is coherent to what has been observed also over Antarctic sea-ice (Nicolaus et al., 2009). Warren et al. (1999) concluded that the average Arctic snow density could reach 320 kg/m³ in May after autumn and winter settling and wind packing.

The statistical analysis of snow density reveals that the sample mean (± std) surface and bulk snow densities observed over the entire MOSAiC period were 311 ± 94 kg/m³ and 291 ± 106 kg/m³, respectively. During the winter-spring period (October–May), the mean (± std) surface and bulk snow densities were 282 ± 77 kg/m³ and 253 ± 59 kg/m³, respectively. The sample average surface (311 kg/m³) and bulk (291 kg/m³) snow densities are comparable to the Arctic snow density climatology reported by Warren et al. (1999), which ranges between 200 and 400 kg/m³. These values are also consistent with Canadian Arctic snow densities, which range from 250 to 350 kg/m³, indicating a long-term consistency in snow properties across the Arctic over decades. These values are also comparable to the mean snow density of about 339 kg/m³ observed over the Antarctic sea-ice (Massom et al., 2001), and specifically to the mean densities of 282 and 356 kg/m³ observed in the Weddell Sea over first-year and second-year ice, respectively (Nicolaus et al. 2009).

Constant snow densities of 348 kg/m³ and 308 kg/m³ were derived from the linear regression of SWE versus snow depth for the entire MOSAiC period and the winter-spring period, respectively. Unlike the density sample statistics, these constant snow densities represent the overall physical relationship between SWE and snow depth, providing a first proxy for snow density in climate modeling.

Finding a robust relationship between bulk snow density samples and air temperature using MOSAiC data remains challenging. Because snow density is affected by wind-driven compaction and wind interaction with surface topography. Snow melting causes simultaneous increases and decreases of density in different snow depths. In addition, snow sampling bias may occur

https://doi.org/10.5194/egusphere-2025-1164
Preprint. Discussion started: 3 April 2025

(Macfarlane et al., 2023a). Similar difficulties in observing a relationship between air temperature and snow density were reported in previous studies conducted in mountainous regions, in the terrestrial Arctic, and over the Greenland ice sheet (Zhao et al., 2023; Howat, 2022). On the other hand, air temperature has been shown to be positively correlated with the fresh snow density in previous studies (Sturm and Holmgren, 1998; Judson and Doesken, 2000). In case of dry snow, air temperature influences the evolution of snow density by the densification process, as it governs the vertical temperature gradients within the snowpack (Zhao et al., 2023). However, over a given period (stage), the impact of air temperature on snow density becomes evident. In Stage III, when temperatures approached 0°C, the mean SSL bulk density reached 503 kg/m³ showing an increasing density from the surface to the bottom of the SSL layer. This contrasts with the bulk snow density of 316 kg/m³ observed during other stages, when air temperatures were significantly colder.

An accumulated wind speed exposure led to an increase in the surface and bulk snow density during stages I and II. The impact of accumulated wind on snow density was strongest, in terms of the regression coefficient, during the first days after a snowfall event. Even after that, the snow density continued to increase with increasing accumulated wind speed, but the slope of the regression decreased. Qualitatively similar relationships were detected in previous campaigns over the Arctic Ocean, Greenland, and the Tibetan Plateau (Zhao et al, 2022; 2023; Howat, 2022). Furthermore, the differential sensitivity of surface and bulk snow densities to accumulated wind speed underscores the importance of temporal scales when considering wind-snow interactions. The effect of wind on surface snow density is more direct than the effect of wind to bulk snow density, which agrees with previous work (Meister, 1989; Sokratov and Sato, 2001; Walter et al., 2024). These findings suggest that future snow modeling efforts should carefully consider the timescale of wind forcing and its interplay with other environmental factors to accurately simulate snow density evolution.

Snow density schemes simulated the gradual increase in snow density during the winter-spring period (Fig. 8). However, none of the snow density parameterizations adequately captured the observed temporal variability. They failed to reproduce the observed decrease in snow density in May. The temporal evolution of snow density influences the thermal conductivity and volumetric heat capacity of snow, which in turn affects the thermal inertia and mass balance of sea ice. Nevertheless, some results from the parameterization schemes (E1, E3, E4(150, 250)) fell within the range of the observed values and align with the snow density climatology of Warren et al. (1999), suggesting their general applicability for sea ice and climate models. On the other hand, snow density has strong spatial variability. King et al. (2020) observed that snow density is highest in thin snow layers over undeformed ice, while is lowest in thicker snow layers over older and deformed ice. Higher densities over thin snow layers are due to the stronger wind compaction over smooth ice, while thicker snow is less dense because of the loose depth hoar bottom. This is associated with the strongest metamorphism occurring when the thick snowpack better insulates the basal layer from the cold winter atmosphere (King et al 2020). Snow density parameterizations capable of addressing spatial variability are needed. Improvements could potentially be achieved through parameterizations based on the probability distribution function (PDF) of snow density (e.g., Liston et al., 2007).

The modeled mean surface temperature (Tsfc), snow temperature (Tsnow), ice temperature (Tice), and ice thickness (Hice) exhibited linearity with mean snow density when applying snow density schemes E1, E2, and E3 with the same initial snow

https://doi.org/10.5194/egusphere-2025-1164
Preprint. Discussion started: 3 April 2025

density. Scheme E4, with different initial snow densities and time series of surface and bulk snow densities, produced another linear trend in these modeled parameters. The temperature and ice thickness differences originating from differences in modeled parameters reached 0.2 °C for Tsfc, 1.4 °C for Tsnow and Tice, and 0.21 m for Hice when applying snow density scheme E1 and ρsfc, despite having the same average snow density (symbols Δ and ∇ in Fig. 9). Snow density and temperature were inversely related: the higher the density, the lower the snow and ice temperatures. Higher snow density leads to a larger snow thermal conductivity, which enhances the heat transfer and increases the impact of the atmospheric forcing on the snowpack. The modelled surface temperature was much less impacted by the snow density. The model runs using a constant snow density showed strong linearity in the modeled snow and ice parameters as snow density increased. This linearity was consistent with that observed in schemes E1–E3. The temporospatial distribution of snow density has a strong connection with snow depth (Key et al., 2020). Additional model experiments revealed nonlinearity in the modeled snow and ice parameters in response to different observed snow water equivalent (SWE) values used as the source term for snow accumulation. By examining Fig. 9 and 10, we can conclude that the response of the modeled snow and ice parameters to the increase in SWE was opposite to their response to the increase in snow density.

High-quality precipitation data could help understand the bulk snow density. The challenges of snowfall data lie largely in the uncertainties of instruments (Matrosov et al. 2022). In this paper, we limited our discussion to surface and bulk snow densities, since these are the primary parameterization options for climate models. For microscale snow density characteristics, more accurate datasets, such as those from SnowMicropen (SMP) and microCT, can be utilized (Macfarlane et al., 2023).

In this study, modeling was conducted exclusively for the winter-spring period because HIGHTSI does not simulate the formation and growth of the surface scattering layer (SSL), which was observed during the MOSAiC melting season. The SSL is a common and widespread feature of Arctic sea ice during the melting season (Smith et al., 2022) and has recently been observed on an Antarctic ice shelf as well (Traversa et al., 2024). However, it is currently not represented in any existing sea ice models or is simulated merely as a persistent snow layer at the top of the ice surface (Smith et al., 2022). This omission or misrepresentation can potentially lead to significant errors in the ice surface energy and mass budgets. To fully understand the formation and melting of the SSL, as well as the associated erosion of the ice surface, a dedicated SSL modeling component should be developed.

Data availability: The ERA5 reanalysis products are available through the Copernicus Climate Data Store portal (https://doi.org/10.24381/cds.adbb2d47, Hersbach et al., 2023). Snow observations available through https://doi.pangaea.de/10.1594/PANGAEA.935934; The precipitation data is publicly available online from the ARM: https://adc.arm.gov/discovery/#/results; The temperature and wind data is available from: https://doi.org/10.18739/A2PV6B83F.

Author contributions: This study was devised by Y.C. and A.R. Initial data retrieval and analyses, as well as draft preparation, were performed by Y.C. B.C. conducted modelling, data analyses, and contributed to draft manuscript preparation and editing. R.P., T.V., W.D., and A.R.M. contributed to draft preparation, results analysis, and editing. R.D., A.R.M., S.A., and M.S. contributed to manuscript editing. All authors participated in the interpretation of the results and manuscript revisions.

https://doi.org/10.5194/egusphere-2025-1164
Preprint. Discussion started: 3 April 2025

Competing interests: At least one of the (co-)authors is a member of the editorial board of The Cryosphere. The authors have no other competing interests to declare.

Acknowledgements: We also acknowledge support by the open-access publication fund of the Alfred-Wegener-Institut, Helmholtz-Zentrum für Polar- und Meeresforschung.

Financial support: Y.C. was funded by the Office of China Postdoctoral Council. Y.C., B.C., R.P., W.D., T.V., and A.R. were funded by the European Union's Horizon 2020 Research and Innovation Programme through the Polar Regions in the Earth System project (PolarRES) under Grant 101003590; S.A. was supported by the Alfred-Wegener-Institut, Helmholtz-Zentrum für Polar- und Meeresforschung, the University of Hamburg, the German Research Foundation's (DFG) projects fAntasie (AR1236/3-1) and SnowCast (AR1236/1-1) within its priority program "Antarctic Research with comparative investigations in the Arctic ice areas" (SPP1158), and the DFG Emmy Noether Programme project SNOWflAke (project number 493362232). A.R.M., R.D. and M.S. were supported by the Swiss Polar Institute (SPI reference DIRCR-2018-003) Funder ID: http://dx.doi.org/10.13039/501100015594. European Union's Horizon 2020 research and innovation program projects ARICE (grant 730965) for berth fees associated with the participation of the DEARice project. WSL Institute for Snow and Avalanche Research SLF. WSL 201812N1678. Funder ID: http://dx.doi.org/10.13039/501100015742 and Swiss National Science Foundation (SNSF) project number P500PN 217845.

Supplement: The supplement related to this article is available online at:

References

Anderson EA.: A point energy and mass balance model of a snow cover, Office of Hydrology, National Weather Service, Maryland, NOAA Technical Report NWS19, 1976.

Bormann, K. J., Westra, S., Evans, J. P., and McCabe, M. F.: Spatial and temporal variability in seasonal snow density, Journal of Hydrology, 484, 63–73, https://doi.org/10.1016/j.jhydrol.2013.01.032, 2013.

Bruland, O., Færevåg, Å., Steinsland, I., Liston, G. E., and Sand, K.: Weather SDM: estimating snow density with high precision using snow depth and local climate, Hydrology Research, 46, 494–506, https://doi.org/10.2166/nh.2015.059, 2015.

Cheng, B., Launiainen, J., and Vihma, T.: Modelling of Superimposed Ice Formation and Sub-Surface Melting in the Baltic Sea, Geophysica, 39, 31–50, 2003.

Cheng, B., Vihma, T., Pirazzini, R., and Granskog, M. A.: Modelling of superimposed ice formation during the spring snowmelt period in the Baltic Sea, Annals of Glaciology, 44, 139–146, https://doi.org/10.3189/172756406781811277, 2006.

Cheng, B., Zhang, Z., Vihma, T., Johansson, M., Bian, L., Li, Z., and Wu, H.: Model experiments on snow and ice thermodynamics in the Arctic Ocean with CHINARE 2003 data, Journal of Geophysical Research: Oceans, 113, https://doi.org/10.1029/2007JC004654, 2008.

Cheng, B., Cheng, Y., Vihma, T., Kontu, A., Zheng, F., Lemmetyinen, J., Qiu, Y., and Pulliainen, J.: Inter-annual variation in lake ice composition in the European Arctic: observations based on high-resolution thermistor strings, Earth System Science Data, 13, 3967–3978, https://doi.org/10.5194/essd-13-3967-2021, 2021.

https://doi.org/10.5194/egusphere-2025-1164
Preprint. Discussion started: 3 April 2025

Derksen, C., Lemmetyinen, J., Toose, P., Silis, A., Pulliainen, J., and Sturm, M.: Physical properties of Arctic versus subarctic snow: Implications for high latitude passive microwave snow water equivalent retrievals, Journal of Geophysical Research: Atmospheres, 119, 7254–7270, https://doi.org/10.1002/2013JD021264, 2014.

Domine, F., Taillandier, A.-S., Houdier, S., Parrenin, F., Simpson, W., and Douglas, T.: Interactions between snow metamorphism and climate: Physical and chemical aspects, Physics and Chemistry of Ice, 2007.

Essery, R., Morin, S., Lejeune, Y., and B Ménard, C.: A comparison of 1701 snow models using observations from an alpine site, Advances in Water Resources, 55, 131–148, https://doi.org/10.1016/j.advwatres.2012.07.013, 2013.

Fausto, R. S., Box, J. E., Vandecrux, B., van As, D., Steffen, K., MacFerrin, M. J., Machguth, H., Colgan, W., Koenig, L. S., McGrath, D., Charalampidis, C., and Braithwaite, R. J.: A Snow Density Dataset for Improving Surface Boundary Conditions in Greenland Ice Sheet Firn Modeling, Front. Earth Sci., 6, https://doi.org/10.3389/feart.2018.00051, 2018.

Fierz, C., Armstrong, R. L., Durand, Y., Etchevers, P., Greene, E., McClung, D. M., Nishimura, K., Satyawali, P. K., and Sokratov S. A.: The International Classification for Seasonal Snow on the Ground, IHP-VII Technical Documents in Hydrology No. 83, IACS Contribution No. 1, UNESCO-IHP, Paris, 2009.

Gong, X., Zhang, J., Croft, B., Yang, X., Frey, M. M., Bergner, N., Chang, R. Y.-W., Creamean, J. M., Kuang, C., Martin, R. V., Ranjithkumar, A., Sedlacek, A. J., Uin, J., Willmes, S., Zawadowicz, M. A., Pierce, J. R., Shupe, M. D., Schmale, J., and Wang, J.: Arctic warming by abundant fine sea salt aerosols from blowing snow, Nat. Geosci., 16, 768–774, https://doi.org/10.1038/s41561-023-01254-8, 2023.

He, S. and Ohara, N.: A New Formula for Estimating the Threshold Wind Speed for Snow Movement, Journal of Advances in Modeling Earth Systems, 9, 2514–2525, https://doi.org/10.1002/2017MS000982, 2017.

Helfricht, K., Hartl, L., Koch, R., Marty, C., and Olefs, M.: Obtaining sub-daily new snow density from automated measurements in high mountain regions, Hydrology and Earth System Sciences, 22, 2655–2668, https://doi.org/10.5194/hess-22-2655-2018, 2018.

Howat, I. M.: Temporal variability in snow accumulation and density at Summit Camp, Greenland ice sheet, Journal of Glaciology, 68, 1076–1084, https://doi.org/10.1017/jog.2022.21, 2022.

Huwald, H., Tremblay, L.-B., and Blatter, H.: Reconciling different observational data sets from Surface Heat Budget of the Arctic Ocean (SHEBA) for model validation purposes, Journal of Geophysical Research: Oceans, 110, https://doi.org/10.1029/2003JC002221, 2005.

Iacozza, J. and Barber, D. G.: An examination of the distribution of snow on sea ‐ ice, Atmosphere-Ocean, 37, 21–51, https://doi.org/10.1080/07055900.1999.9649620, 1999.

Itkin, P., Hendricks, S.,Webster, M., von Albedyll, L., Arndt, S., Divine, D., Jaggi, M., Oggier, M., Raphael, I., Ricker, R., Rohde, J., Schneebeli, M., and Liston, G. E.: Sea ice and snow characteristics from year-long transects at the MOSAiC Central Observatory, Elementa: Science of the Anthropocene, 11, 00 048, https://doi.org/10.1525/elementa.2022.00048, https://doi.org/10.1525/elementa.2022.00048, 2023.

https://doi.org/10.5194/egusphere-2025-1164
Preprint. Discussion started: 3 April 2025

Itkin, P. and Liston, G. E.: Combining observational data and numerical models to obtain a seamless high temporal resolution seasonal cycle of snow and ice mass balance at the MOSAiC Central Observatory, EGUsphere, 1–36, https://doi.org/10.5194/egusphere-2024-3402, 2024.

Jafari, M., Gouttevin, I., Couttet, M., Wever, N., Michel, A., Sharma, V., Rossmann, L., Maass, N., Nicolaus, M., and Lehning, M.: The Impact of Diffusive Water Vapor Transport on Snow Profiles in Deep and Shallow Snow Covers and on Sea Ice, Frontiers in Earth Science, 8, https://doi.org/10.3389/feart.2020.00249, 2020.

Judson, A. and Doesken, N.: Density of Freshly Fallen Snow in the Central Rocky Mountains, Bulletin of the American Meteorological Society, 81, 1577–1588, https://doi.org/10.1175/1520-0477(2000)081<1577:DOFFSI>2.3.CO;2, 2000.

Keenan, E., Wever, N., Dattler, M., Lenaerts, J. T. M., Medley, B., Kuipers Munneke, P., and Reijmer, C.: Physics-based SNOWPACK model improves representation of near-surface Antarctic snow and firn density, The Cryosphere, 15, 1065–1085, https://doi.org/10.5194/tc-15-1065-2021, 2021.

Kern, S., Khvorostovsky, K., Skourup, H., Rinne, E., Parsakhoo, Z. S., Djepa, V., Wadhams, P., and Sandven, S.: The impact of snow depth, snow density and ice density on sea ice thickness retrieval from satellite radar altimetry: results from the ESA-CCI Sea Ice ECV Project Round Robin Exercise, The Cryosphere, 9, 37–52, https://doi.org/10.5194/tc-9-37-2015, 2015.

King, J., Howell, S., Brady, M., Toose, P., Derksen, C., Haas, C., and Beckers, J.: Local-scale variability of snow density on Arctic sea ice, The Cryosphere, 14, 4323–4339, https://doi.org/10.5194/tc-14-4323-2020, 2020.

Koo, Y., Lei, R., Cheng, Y., Cheng, B., Xie, H., Hoppmann, M., Kurtz, N. T., Ackley, S. F., and Mestas-Nuñez, A. M.: Estimation of thermodynamic and dynamic contributions to sea ice growth in the Central Arctic using ICESat-2 and MOSAiC SIMBA buoy data, Remote Sensing of Environment, 267, 112730, https://doi.org/10.1016/j.rse.2021.112730, 2021.

Launiainen, J. and Cheng, B.: Modelling of ice thermodynamics in natural water bodies, Cold Regions Science and Technology, 27, 153–178, https://doi.org/10.1016/S0165-232X(98)00009-3, 1998.

Leeuw, N. de, Birkeland, K., and Hendrikx, J.: UNDERSTANDING METEOROLOGICAL CONTROLS ON WIND SLAB PROPERTIES, International Snow Science Workshop Proceedings 2023, Bend, Oregon, 1104–1111, 2023.

Liston, G. E., Haehnel, R. B., Sturm, M., Hiemstra, C. A., Berezovskaya, S., and figr, R. D.: Simulating complex snow distributions in windy environments using SnowTran-3D, Journal of Glaciology, 53, 241–256, https://doi.org/10.3189/172756507782202865, 2007.

Macfarlane, A. R., Schneebeli, M., Dadic, R., Wagner, D. N., Arndt, S., Clemens-Sewall, D., Hämmerle, S., Hannula, H.-R., Jaggi, M., Kolabutin, N., Krampe, D., Lehning, M., Matero, I., Nicolaus, M., Oggier, M., Pirazzini, R., Polashenski, C., Raphael, I., Regnery, J., Shimanchuck, E., Smith, M. M., and Tavri, A.: Snowpit raw data collected during the MOSAiC expedition, https://doi.org/10.1594/PANGAEA.935934, 2021.

Macfarlane, A. R., Schneebeli, M., Dadic, R., et al.: A Database of Snow on Sea Ice in the Central Arctic Collected during the MOSAiC expedition, Sci Data, 10, 398, https://doi.org/10.1038/s41597-023-02273-1, 2023a.

https://doi.org/10.5194/egusphere-2025-1164
Preprint. Discussion started: 3 April 2025

Macfarlane, A. R., Dadic, R., Smith, M. M., Light, B., Nicolaus, M., Henna-Reetta, H., Webster, M., Linhardt, F., Hämmerle, S., and Schneebeli, M.: Evolution of the microstructure and reflectance of the surface scattering layer on melting, level Arctic sea ice, Elementa: Science of the Anthropocene, 11, 00103, https://doi.org/10.1525/elementa.2022.00103, 2023b.

Macfarlane, A. R., Löwe, H., Gimenes, L., Wagner, D. N., Dadic, R., Ottersberg, R., Hämmerle, S., and Schneebeli, M.: Thermal Conductivity of Snow on Arctic Sea Ice, EGUsphere, 1–22, https://doi.org/10.5194/egusphere-2023-83, 2023c.

Massom, R. A., Eicken, H., Hass, C., Jeffries, M. O., Drinkwater, M. R., Sturm, M., Worby, A. P., Wu, X., Lytle, V. I., Ushio, S., Morris, K., Reid, P. A., Warren, S. G., and Allison, I.: Snow on Antarctic sea ice, Reviews of Geophysics, 39, 413–445, https://doi.org/10.1029/2000RG000085, 2001.

Matrosov, S. Y., Shupe, M. D., and Uttal, T.: High temporal resolution estimates of Arctic snowfall rates emphasizing gauge and radar-based retrievals from the MOSAiC expedition, Elementa: Science of the Anthropocene, 10, 00101, https://doi.org/10.1525/elementa.2021.00101, 2022.

McCreight, J. L. and Small, E. E.: Modeling bulk density and snow water equivalent using daily snow depth observations, The Cryosphere, 8, 521–536, https://doi.org/10.5194/tc-8-521-2014, 2014.

Meister, R.: Influence of Strong Winds on Snow Distribution and Avalanche Activity, Annals of Glaciology, 13, 195–201, https://doi.org/10.3189/S0260305500007886, 1989.

Menard, C. B., Essery, R., Krinner, G., et al.: Scientific and Human Errors in a Snow Model Intercomparison, Bulletin of the American Meteorological Society, 102, E61–E79, https://doi.org/10.1175/BAMS-D-19-0329.1, 2021.

Merkouriadi, I., Gallet, J.-C., Graham, R. M., Liston, G. E., Polashenski, C., Rösel, A., and Gerland, S.: Winter snow conditions on Arctic sea ice north of Svalbard during the Norwegian young sea ICE (N-ICE2015) expedition, Journal of Geophysical Research: Atmospheres, 122, 10,837-10,854, https://doi.org/10.1002/2017JD026753, 2017.

Merkouriadi, I., Liston, G. E., Graham, R. M., and Granskog, M. A.: Quantifying the Potential for Snow-Ice Formation in the Arctic Ocean, Geophysical Research Letters, 47, e2019GL085020, https://doi.org/10.1029/2019GL085020, 2020.

Mizukami, N. and Perica, S.: Spatiotemporal Characteristics of Snowpack Density in the Mountainous Regions of the Western United States, Journal of Hydrometeorology, 9, 1416–1426, 2008.

Nicolaus, M., Haas, C. and S. Willmes S.: Evolution of first-year and second-year snow properties on sea ice in the Weddell Sea during spring-summer transition, J. Geophys. Res., 114, D17109, doi:10.1029/2008JD011227, 2009.

Nicolaus, M., Perovich, D. K., Spreen, G., et al.: Overview of the MOSAiC expedition: Snow and sea ice, Elementa: Science of the Anthropocene, 10, 000046, https://doi.org/10.1525/elementa.2021.000046, 2022.

Perovich, D. K. and Polashenski, C.: Albedo evolution of seasonal Arctic sea ice, Geophysical Research Letters, 39, https://doi.org/10.1029/2012GL051432, 2012.

Pielmeier, C. and Schneebeli, M.: Stratigraphy and changes in hardness of snow measured by hand, ramsonde and snow micro penetrometer: A comparison with planar sections, Cold Regions Science and Technology - COLD REG SCI TECHNOL, 37, 393–405, https://doi.org/10.1016/S0165-232X(03)00079-X, 2003.

https://doi.org/10.5194/egusphere-2025-1164
Preprint. Discussion started: 3 April 2025

Pirazzini, R., Vihma, T., Granskog, M. A., and Cheng, B.: Surface albedo measurements over sea ice in the Baltic Sea during the spring snowmelt period, Annals of Glaciology, 44, 7–14, https://doi.org/10.3189/172756406781811565, 2006.

Pistocchi, A.: Simple estimation of snow density in an Alpine region, Journal of Hydrology: Regional Studies, 6, 82–89, https://doi.org/10.1016/j.ejrh.2016.03.004, 2016.

Pringle, D. J., Eicken, H., Trodahl, H. J., and Backstrom, L. G. E.: Thermal conductivity of landfast Antarctic and Arctic sea ice, Journal of Geophysical Research: Oceans, 112, https://doi.org/10.1029/2006JC003641, 2007.

Proksch, M., Rutter, N., Fierz, C., and Schneebeli, M.: Intercomparison of snow density measurements: bias, precision, and vertical resolution, The Cryosphere, 10, 371–384, https://doi.org/10.5194/tc-10-371-2016, 2016.

Provost, C., Sennéchael, N., Miguet, J., Itkin, P., Rösel, A., Koenig, Z., Villacieros-Robineau, N., and Granskog, M. A.: Observations of flooding and snow-ice formation in a thinner Arctic sea-ice regime during the N-ICE2015 campaign: Influence of basal ice melt and storms, Journal of Geophysical Research: Oceans, 122, 7115–7134, https://doi.org/10.1002/2016JC012011, 2017.

Rabe, B., Heuzé, C., Regnery, J., et al: Overview of the MOSAiC expedition: Physical oceanography, Elementa: Science of the Anthropocene, 10, 00062, https://doi.org/10.1525/elementa.2021.00062, 2022.

Saloranta, T.: Modelling the evolution of snow, snow ice and ice in the Baltic Sea, Tellus 52A, 93-108, 2000.

Seligman, G.: Snow structure and ski fields: being an account of snow and ice forms met with in nature, and a study on avalanches and snowcraft, Macmillan and Co., London, 555 pp., 1936.

Shupe, MD, Rex, M, Dethloff, K, Damm, E, Fong, AA, Gradinger, R, Heuze´, C, Loose, B, Makarov, A, Maslowski, W, Nicolaus, M, Perovich, D, Rabe, B, Rinke, A, Sokolov, V, Sommerfeld, A.: The MOSAiC expedition: A year drifting with the Arctic sea ice, Arctic Report Card, http://dx.doi.org/10.25923/9g3v-xh92, 2020.

Shupe, M. D., Rex, M., Blomquist, B., et al.: Overview of the MOSAiC expedition: Atmosphere, Elementa: Science of the Anthropocene, 10, 00060, https://doi.org/10.1525/elementa.2021.00060, 2022.

Sigmund, A., Dujardin, J., Comola, F., Sharma, V., Huwald, H., Melo, D. B., Hirasawa, N., Nishimura, K., and Lehning, M.: Evidence of Strong Flux Underestimation by Bulk Parametrizations During Drifting and Blowing Snow, Boundary Layer Meteorol, 182, 119–146, https://doi.org/10.1007/s10546-021-00653-x, 2022.

Smith, M. M., Light, B., Macfarlane, A. R., Perovich, D. K., Holland, M. M., and Shupe, M. D.: Sensitivity of the Arctic Sea Ice Cover to the Summer Surface Scattering Layer, Geophysical Research Letters, 49, e2022GL098349, https://doi.org/10.1029/2022GL098349, 2022.

Sokratov, S. A. and Sato, A.: The effect of wind on the snow cover, Annals of Glaciology, 32, 116–120, https://doi.org/10.3189/172756401781819436, 2001.

Sommerfeld, R. A. and LaChapelle, E.: The Classification of Snow Metamorphism, Journal of Glaciology, 9, 3–18, https://doi.org/10.3189/S0022143000026757, 1970.

Stroeve, J., Nandan, V., Willatt, R., Dadic, R., Rostosky, P., Gallagher, M., Mallett, R., Barrett, A., Hendricks, S., Tonboe, R., McCrystall, M., Serreze, M., Thielke, L., Spreen, G., Newman, T., Yackel, J., Ricker, R., Tsamados, M., Macfarlane, A.,

https://doi.org/10.5194/egusphere-2025-1164
Preprint. Discussion started: 3 April 2025

Hannula, H.-R., and Schneebeli, M.: Rain on snow (ROS) understudied in sea ice remote sensing: a multi-sensor analysis of ROS during MOSAiC (Multidisciplinary drifting Observatory for the Study of Arctic Climate), The Cryosphere, 16, 4223–4250, https://doi.org/10.5194/tc-16-4223-2022, 2022.

Sturm, M. and Holmgren, J.: Differences in compaction behavior of three climate classes of snow, Annals of Glaciology, 26, 125–130, https://doi.org/10.3189/1998AoG26-1-125-130, 1998.

Sturm, M., Holmgren, J., König, M., and Morris, K.: The thermal conductivity of seasonal snow, Journal of Glaciology, 43, 26–41, https://doi.org/10.3189/s0022143000002781, 1997.

Sturm, M., Perovich, D. K., and Holmgren, J.: Thermal conductivity and heat transfer through the snow on the ice of the Beaufort Sea, Journal of Geophysical Research: Oceans, 107, SHE 19-1-SHE 19-17, https://doi.org/10.1029/2000JC000409, 2002.

Sturm, M., Taras, B., Liston, G. E., Derksen, C., Jonas, T., and Lea, J.: Estimating Snow Water Equivalent Using Snow Depth Data and Climate Classes, Journal of Hydrometeorology, 11, 1380–1394, https://doi.org/10.1175/2010JHM1202.1, 2010.

Svensson, G. , Murto, S. , Shupe, M. D. , Pithan, F. , Magnusson, L. , Day, J. J. , Doyle, J. D. , Renfrew, I. A. , Spengler, T. and Vihma, T.: Warm air intrusions reaching the MOSAiC expedition in April 2020—The YOPP targeted observing period (TOP) , Elementa: Science of the Anthropocene, 11 (1) . doi: 10.1525/elementa.2023.00016, 2023.

Szeitz, A. J. and Moore, R. D.: Modelling snowpack bulk density using snow depth, cumulative degree-days, and climatological predictor variables, Hydrological Processes, 37, e14800, https://doi.org/10.1002/hyp.14800, 2023.

Wagner, D. N., Shupe, M. D., Cox, C., Persson, O. G., Uttal, T., Frey, M. M., Kirchgaessner, A., Schneebeli, M., Jaggi, M., Macfarlane, A. R., Itkin, P., Arndt, S., Hendricks, S., Krampe, D., Nicolaus, M., Ricker, R., Regnery, J., Kolabutin, N., Shimanshuck, E., Oggier, M., Raphael, I., Stroeve, J., and Lehning, M.: Snowfall and snow accumulation during the MOSAiC winter and spring seasons, The Cryosphere, 16, 2373–2402, https://doi.org/10.5194/tc-16-2373-2022, 2022.

Wang, C., Cheng, B., Wang, K., Gerland, S., and Pavlova, O.: Modelling snow ice and superimposed ice on landfast sea ice in Kongsfjorden, Svalbard, Polar Research, https://doi.org/10.3402/polar.v34.20828, 2015.

Warren, S. G., Rigor, I. G., Untersteiner, N., Radionov, V. F., Bryazgin, N. N., Aleksandrov, Y. I., and Colony, R.: Snow Depth on Arctic Sea Ice, Journal of Climate, 12, 1814–1829, https://doi.org/10.1175/1520-0442(1999)012<1814:SDOASI>2.0.CO;2, 1999.

Yen, Y.-C.: Review of thermal properties of snow, ice and sea ice, This Digital Resource was created from scans of the Print Resource, Cold Regions Research and Engineering Laboratory (U.S.), 1981.

Zhao, D., Chen, S., Chen, Y., Gong, Y., Lou, G., Cheng, S., and Bi, H.: Influence of Dust Aerosols on Snow Cover Over the Tibetan Plateau, Front. Environ. Sci., 10, https://doi.org/10.3389/fenvs.2022.839691, 2022.

Zhao, W., Mu, C., Han, L., Sun, W., Sun, Y., and Zhang, T.: Spatial and temporal variability in snow density across the Northern Hemisphere, CATENA, 232, 107445, https://doi.org/10.1016/j.catena.2023.107445, 2023.